INJURY BIOMECHANICS RESEARCH
Proceedings of the Thirty-Seventh International Workshop

Measurement of 3-D Head Kinematics in Impact Conditions Employing Six-Accelerometers and Three-Angular Rate Sensors (6aω Configuration)

Y. Kang, K. Moorhouse and J. H. Bolte IV

ABSTRACT

The ability to measure 3-D head kinematics in motor vehicle crash conditions is important for assessing head-neck loads as well as brain injuries. A method for obtaining accurate 3-D head kinematics of post mortem human subjects (PMHS) in short duration impact conditions is proposed and validated in this study. The proposed methodology utilizes six accelerometers and three angular rate sensors (6aω configuration) such that an algebraic equation is used to determine angular acceleration with respect to the body-fixed coordinate system, and angular velocity is measured directly rather than numerically integrating the angular acceleration. Head impact tests to validate the method were conducted using the internal nine accelerometer head of the Hybrid III dummy and the proposed 6aω scheme in both low (2.3 m/s) and high (4.0 m/s) speed impact conditions. A rear impact sled test (10.5g and 24 km/h) using the Hybrid III dummy was also conducted to validate the 6aω scheme on a tetrahedron fixture which can be installed on the head of a PMHS. For both test conditions, the 6aω method was compared with a nine accelerometer array sensor package (NAP) as well as a configuration of three accelerometers and three angular rate sensors (3aω), both of which have been commonly used to measure 3-D kinematics of the head for assessment of brain and neck injuries. The ability of each of the three methods (6aω, 3aω, and NAP) to accurately measure 3-D head kinematics was quantified by calculating the normalized root mean squared deviation (NRMSD), which provides an average percent error over time. Results from the head impact tests indicate that angular acceleration obtained from the 6aω scheme was comparable to that determined from the NAP scheme, while angular acceleration derived from the 3aω scheme was not accurate in the high speed head impact condition. Results from the rear impact sled test indicate that all three schemes (NAP, 3aω and 6aω) provide

accurate linear acceleration in the body-fixed coordinate system on the head as well as in the global coordinate system, while the 6aω and 3aω scheme produce more accurate results for the angular displacement (rotation) in the global coordinate system than the NAP scheme. Overall the proposed 6aω scheme provides more accurate kinematics in the global coordinate system and a more accurate transformation matrix at each time step, since the error due to numerical integration and numerical differentiation is minimized in the transformation of head kinematics to the global (inertial) coordinate system.

INTRODUCTION

Techniques for measuring three dimensional (3-D) head kinematics of post mortem human subjects (PMHS) and anthropomorphic test devices (ATDs) have been developed and evaluated extensively (Becker and Willems, 1975; Ewing et al., 1975; Krieger et al., 1976; Ewing et al., 1977a; Ewing et al., 1977b; Padgaonkar et al., 1975; Nusholtz et al., 1986; Viano et al., 1986; Laughlin, 1989; Bendjellal et al., 1990; Bendjellal et al., 1992; Nusholtz, 1993; DiMasi, 1995a; DiMasi, 1995b; Martin et al., 1997; Martin et al., 1998). Theoretically, six degree of freedom rigid body kinematics can be determined using only six accelerometers, and several studies have utilized this methodology (Becker and Willems, 1975; Ewing et al., 1975; Ewing et al., 1977a; Ewing et al., 1977b). Becker and Willems (1975) developed a 'T' shaped fixture for employing six accelerometers which was used for measuring the 3-D kinematics of the head, first thoracic vertebra, and pelvis in Ewing et al.'s volunteer sled tests (Ewing et al., 1975; Ewing et al., 1977a; Ewing et al., 1977b). Although the six accelerometer method is theoretically feasible for measuring 3-D kinematics, three nonlinear ordinary differential equations must be solved numerically in order to obtain angular acceleration and velocity, and this numerical procedure has been reported as being mathematically unstable and inapplicable to severe impact conditions (Padgaonkar et al., 1975). Therefore, in order to avoid the unstable computational procedure using only six accelerometers, many efforts have been made to develop and validate new instrumentation schemes for measuring 3-D kinematics of the ATD and PMHS head. Examples of such instrumentation schemes include nine accelerometer array packages in either a 3-2-2-2 array (Padgaonkar et al., 1975) or 3-3-3 array (Nusholtz, 1993), an in-line accelerometer package using 15 accelerometers (Viano et al., 1986), a multi-accelerometer approach using 12 accelerometers (Bendjellal et al., 1990), utilization of three accelerometers and three angular rate sensors (Laughlin, 1989; Martin et al., 1997), and peripheral schemes using six and/or nine accelerometers with three angular rate sensors (Martin et al., 1998).

The most frequently implemented method to obtain 3-D head kinematics is the 3-2-2-2 nine accelerometer array package (NAP) (Padgaonkar et al., 1975). The NAP scheme installed on various instrumentation fixtures attached to the PMHS head (e.g. triangular pyramidal fixture (Yoganandan et al., 2006) and tetrahedral fixture (Hardy et al., 2007)) has been utilized for the assessment of brain injuries and measurement of head-neck kinematics (Hardy et al., 2001; Hardy et al., 2007; Takhounts et al., 2003; Deng et al., 2000; Kallieris et al., 1996). An advantage of the NAP scheme is that angular acceleration with respect to the head's body-fixed coordinate system can be determined from algebraic equations using the accelerometer data without numerical differentiation (Padgaonkar et al., 1975). Accurate angular accelerations are important for calculating the linear acceleration at an inaccessible point, such as the center of gravity (CG) of the head in PMHS tests, which is commonly required to evaluate head injuries (e.g. head injury criteria, HIC). Even though the NAP scheme has been reported as the most reliable method to produce accurate 3-D kinematics of the head (Padgaonkar et al., 1975; Yoganandan et al., 2006), numerical integration required to obtain velocities and displacements of the head may be a drawback of the NAP scheme due to accumulation of error (Nusholtz, 1993; Martin et al., 1998; Deng et al., 2000), particularly with regard to the double numerical integration required for displacements.

Angular rate sensors combined with accelerometers provide another way to measure 3-D kinematics of the head, and have been used in multiple impact experiments (Martin et al., 1997; Martin et al., 1998; Yoganandan et al., 2000). These studies have investigated various configurations of accelerometers and angular rate sensors including a 3aω scheme using three accelerometers with three magnetohydrodynamic

(MHD) angular rate sensors (Martin et al., 1997), and a peripheral scheme using six and/or nine accelerometers with three MHD angular rate sensors (Martin et al., 1998). These schemes theoretically produce accurate angular velocity and angular displacement since angular velocity is directly measured by the angular rate sensors, and only single numerical integration is required for angular displacement. This notion is supported experimentally in Martin et al. (1997) where they found that the 3aω scheme (called Dynacube in the paper) was capable of measuring accurate angular velocity as compared with theoretical responses and potentiometer data in a torsional pendulum test. However, a significant drawback of the 3aω scheme (where only three accelerometers are employed) is that the angular acceleration can only be obtained by numerically differentiating the angular rate sensor data, resulting in noisy signals.

Martin et al. (1998) developed a peripheral scheme using six and/or nine accelerometers with three MHD angular rate sensors, and directly compared the results to the NAP scheme. In this study, MHD angular rate sensors and three triaxial accelerometer clusters were installed on the anterior, lateral, and superior aspects of the surface or periphery of the Hybrid III head, such that the local coordinate systems on the three triaxial accelerometer clusters were precisely aligned along the pre-defined body-fixed coordinate system of the head. Six of the nine accelerometers and three angular rate sensors could then be used to determine the angular acceleration of the head using algebraic equations, and angular velocity could be measured directly by the angular rate sensors. Therefore this peripheral scheme resolves both the issue in the NAP scheme involving numerical integration of angular acceleration to obtain angular velocity, and the issue in the 3aω scheme involving numerical differentiation of angular velocity to determine angular acceleration. Although using only six of the nine accelerometers is sufficient for the ATD head (where the local coordinate system on each cluster can be precisely aligned with the body-fixed coordinate system at the head CG), determining locations for the triaxial accelerometer clusters on the PMHS head that are both parallel and orthogonal to the body-fixed coordinate system at the head CG is difficult. Furthermore, even if the precise location for the clusters was determined, parallelism of the three clusters can be lost when there is local deformation of the PMHS head during high speed head impacts, so the periphery scheme using only six accelerometers would be limited to low severity tests. Therefore, for the PMHS head three additional accelerometers are required to avoid the parallelism and orthogonality constraints described above, making the total number of sensors required for measurement of 3-D PMHS head kinematics using the peripheral scheme to be twelve (nine accelerometers and three angular rate sensors). A final limitation of this method is that the instrumentation must be installed at three different places on the head (e.g., vertex of the skull, temporo-parietal region, and occipital region) so there exists a high risk of sensor damage due to contact with external structures during the event. Martin et al. (1998) also introduced a theoretical co-planar scheme using six accelerometers and three angular rate sensors installed on a single flat plate fixture, although this scheme was not evaluated experimentally.

The objective of this study is to propose and validate an improved head instrumentation scheme capable of measuring 3-D kinematics using six accelerometers and three angular rate sensors (6aω) installed on a single tetrahedron fixture. This 6aω scheme will allow for PMHS to be tested in both direct impact and non-impact environments at all severities, while capturing accurate 3-D kinematics of the head in both the body-fixed coordinate system and in the lab or global coordinate system. The kinematic data obtained from the 6aω scheme should aid in the development and evaluation of injury criteria of the head.

METHODS

3-D kinematics of a rigid body

Regardless of the instrumentation technique or configuration chosen to measure 3-D head kinematics, the underlying equations of motion for the head, assumed to be a rigid body, remain the same. Below is a brief development of these equations, and a full detailed procedure for the analysis of rigid-body kinematics can be found in the references (Nikravesh, 1985; Nikravesh, 1988).

Position analysis. A vector expression of an arbitrary point P on a rigid body shown in Figure 1 can be expressed as:

$$\underline{\mathbf{r}}^{\mathbf{P}} = \underline{\mathbf{r}} + \underline{\mathbf{s}}^{\mathbf{P}} \tag{1}$$

where: $\underline{\mathbf{r}}^{\mathbf{P}} = [x^P, y^P, z^P]^T$ are the global coordinates of the point P

$\underline{\mathbf{r}} = [x, y, z]^T$ are the global coordinates of the origin of the body-fixed coordinate system

$\underline{\mathbf{s}}^{\mathbf{P}}$ is a vector from the origin of the body-fixed coordinate system to the point P with respect to the global coordinate system.

Equation (1) can be rewritten as:

$$\underline{\mathbf{r}}^{\mathbf{P}} = \underline{\mathbf{r}} + \underline{\mathbf{A}\mathbf{s}'^{\mathbf{P}}} \tag{2}$$

where: $\underline{\mathbf{s}'^{\mathbf{P}}} = [x'^P, y'^P, z'^P]^T$ are the local (body-fixed) coordinates of the point P on the rigid body

$\underline{\mathbf{A}}$ is a transformation matrix using time-dependent Euler angles or Euler parameters (Nikravesh, 1988). See Appendix A for details regarding the procedure used in this study for generating the 2-1-3 Euler angle transformation matrix and updating it at each time point.

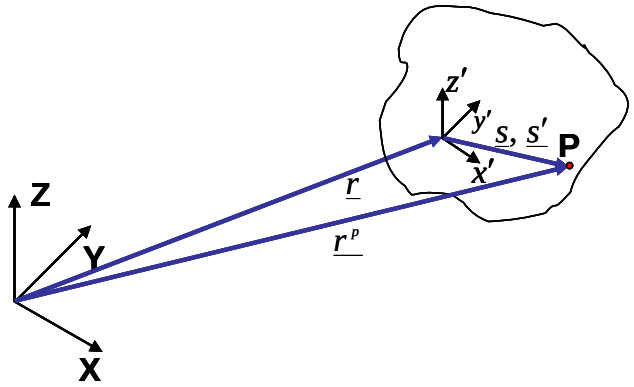

Figure 1: Global coordinate system (XYZ) and body-fixed (moving frame) coordinate system (x´y´z´)

Velocity analysis. Equation (2) can be differentiated with respect to time to obtain the velocity equation:

$$\dot{\underline{\mathbf{r}}}^{\mathbf{P}} = \dot{\underline{\mathbf{r}}} + \dot{\underline{\mathbf{A}}}\underline{\mathbf{s}'^{\mathbf{P}}} + \underline{\mathbf{A}}\dot{\underline{\mathbf{s}}}'^{\mathbf{P}} \tag{3}$$

where: $\dot{\underline{\mathbf{A}}} = \underline{\tilde{\boldsymbol{\omega}}\mathbf{A}} = \mathbf{A}\underline{\tilde{\boldsymbol{\omega}}'}$, the tilda (skew-symmetric matrix) represents the cross product, and the third term is zero for a rigid body.

Substituting $\dot{\underline{\mathbf{A}}} = \mathbf{A}\underline{\tilde{\boldsymbol{\omega}}'}$ into Equation (3) it can be rewritten as:

$$\dot{\underline{\mathbf{r}}}^{\mathbf{P}} = \dot{\underline{\mathbf{r}}} + \underline{\mathbf{A}\tilde{\boldsymbol{\omega}}'\mathbf{s}'^{\mathbf{P}}} \tag{4}$$

Acceleration analysis. Equation (2) may be differentiated twice with respect to time to obtain the following equation for acceleration:

$$\ddot{\underline{\mathbf{r}}}^{\mathbf{P}} = \ddot{\underline{\mathbf{r}}} + \ddot{\underline{\mathbf{A}}}\underline{\mathbf{s}'^{\mathbf{P}}} \tag{5}$$

where: $\ddot{\underline{\mathbf{A}}} = \underline{\dot{\tilde{\boldsymbol{\omega}}}\mathbf{A}} + \underline{\tilde{\boldsymbol{\omega}}\tilde{\boldsymbol{\omega}}\mathbf{A}} = \underline{\mathbf{A}\dot{\tilde{\boldsymbol{\omega}}}'} + \underline{\mathbf{A}\tilde{\boldsymbol{\omega}}'\tilde{\boldsymbol{\omega}}'}$

Substituting $\ddot{\underline{\mathbf{A}}} = \underline{\mathbf{A}\dot{\tilde{\boldsymbol{\omega}}}'} + \underline{\mathbf{A}\tilde{\boldsymbol{\omega}}'\tilde{\boldsymbol{\omega}}'}$ into Equation (5), the acceleration equation can be written as:

$$\ddot{\underline{\mathbf{r}}}^{\mathbf{P}} = \ddot{\underline{\mathbf{r}}} + \underline{\mathbf{A}\dot{\tilde{\boldsymbol{\omega}}}'\mathbf{s}'^{\mathbf{P}}} + \underline{\mathbf{A}\tilde{\boldsymbol{\omega}}'\tilde{\boldsymbol{\omega}}'\mathbf{s}'^{\mathbf{P}}} \tag{6}$$

It should be noted that Equations (2), (4), and (6) represent the displacement, velocity, and acceleration, respectively, of P in the global coordinate system, not in the body-fixed coordinate system which is continually moving. To transform these equations from the global coordinate system to the local body-fixed coordinate system, they can be pre-multiplied by the transpose of the transformation matrix, $\underline{\mathbf{A}^{\mathbf{T}}}$. The equations for velocity and acceleration in the body-fixed coordinate system can then be expressed as:

$$\dot{\underline{\mathbf{r}}}'^{\mathbf{P}} = \dot{\underline{\mathbf{r}}}' + \underline{\tilde{\boldsymbol{\omega}}'\mathbf{s}'^{\mathbf{P}}} \tag{7}$$

$$\ddot{\underline{\mathbf{r}}}'^{\mathbf{P}} = \ddot{\underline{\mathbf{r}}}' + \underline{\dot{\tilde{\boldsymbol{\omega}}}'\mathbf{s}'^{\mathbf{P}}} + \underline{\tilde{\boldsymbol{\omega}}'\tilde{\boldsymbol{\omega}}'\mathbf{s}'^{\mathbf{P}}} \tag{8}$$

where: $\dot{\underline{\mathbf{r}}}'^{\mathbf{P}}$ and $\ddot{\underline{\mathbf{r}}}'^{\mathbf{P}}$ are vectors for velocity and acceleration of a point P with respect to the body-fixed (moving frame) coordinate system, respectively.

NAP, 3aω, and 6aω schemes

Of the numerous instrumentation techniques and configurations described earlier for measuring 3-D head kinematics, two of the commonly used schemes (NAP and 3aω) were chosen in this study for direct comparison with the 6aω scheme developed herein. In the measurement of 3-D head kinematics, one of the most important considerations is to ensure that accurate angular accelerations are obtained. One method for doing so is to use a nine-accelerometer package (NAP, 3-2-2-2) developed by Padgaonker et al. (1975), which has been widely used in a variety of impact conditions within the literature (Yoganandan et al., 2006; Hardy et al., 2001; Hardy et al., 2007; Takhounts et al., 2003; Deng et al., 2000; Kallieris et al., 1996). An illustration of the NAP scheme is shown in Figure 2(a) with each of the nine accelerometers indicated in red in a 3-2-2-2 array. It is important to note that the individual accelerometer terms denoted by an italicized A with subscripts should not be confused with the bold-faced and underlined transformation matrix $\underline{\mathbf{A}}$. Equation (8) can be used to derive the angular acceleration for this instrumentation configuration. Beginning with point b in Figure 2(a), Equation (8) can be rewritten as:

$$\underline{\ddot{\mathbf{r}}}'^{\mathbf{b}} = \underline{\ddot{\mathbf{r}}}'^{\mathbf{o}} + \underline{\tilde{\dot{\boldsymbol{\omega}}}}'\underline{\mathbf{s}}'^{\mathbf{b}} + \underline{\tilde{\boldsymbol{\omega}}}'\underline{\tilde{\boldsymbol{\omega}}}'\underline{\mathbf{s}}'^{\mathbf{b}} \tag{9}$$

where: $\underline{\ddot{\mathbf{r}}}'^{\mathbf{b}} = [A_{bx'}, A_{by'}, A_{bz'}]^T$, $\underline{\ddot{\mathbf{r}}}'^{\mathbf{o}} = [A_{0x'}, A_{0y'}, A_{0z'}]^T$, and $\underline{\mathbf{s}}'^{\mathbf{b}} = [0, \rho_{by'}, 0]^T$.

Equation (9) can then be separated into x- and z- vector components as shown in Equations (10) and (11):

$$A_{bx'} = A_{0x'} + \omega_{x'}\,\omega_{y'}\rho_{by'} - \dot{\omega}_{z'}\rho_{by'} \tag{10}$$

$$A_{bz'} = A_{0z'} + \omega_{y'}\,\omega_{z'}\rho_{by'} + \dot{\omega}_{x'}\rho_{by'} \tag{11}$$

Note that the y-vector component of Equation (9) is not analyzed since acceleration is not measured in the y-direction at point b.

Equations (10) and (11) can now be expressed in terms of the desired angular accelerations as shown in Equations (12) and (13):

$$\dot{\omega}_{z'} = (A_{0x'} - A_{bx'})/\rho_{by'} + \omega_{x'}\omega_{y'} \tag{12}$$

$$\dot{\omega}_{x'} = -(A_{0z'} - A_{bz'})/\rho_{by'} - \omega_{y'}\omega_{z'} \tag{13}$$

Following a similar procedure for points a and c yields Equations (14)-(21):

$$A_{ay'} = A_{0y'} + \omega_{x'}\,\omega_{y'}\rho_{ax'} + \dot{\omega}_{z'}\rho_{ax'} \tag{14}$$

$$\dot{\omega}_{z'} = -(A_{0y'} - A_{ay'})/\rho_{ax'} - \omega_{x'}\omega_{y'} \tag{15}$$

$$A_{az'} = A_{0z'} + \omega_{x'}\,\omega_{z'}\rho_{ax'} - \dot{\omega}_{y'}\rho_{ax'} \tag{16}$$

$$\dot{\omega}_{y'} = (A_{0z'} - A_{az'})/\rho_{ax'} + \omega_{x'}\omega_{z'} \tag{17}$$

$$A_{cx'} = A_{0x'} + \omega_{x'}\,\omega_{z'}\rho_{cz'} + \dot{\omega}_{y'}\rho_{cz'} \tag{18}$$

$$\dot{\omega}_{y'} = -(A_{0x'} - A_{cx'})/\rho_{cz'} - \omega_{x'}\omega_{z'} \tag{19}$$

$$A_{cy'} = A_{0y'} + \omega_{y'}\,\omega_{z'}\rho_{cz'} - \dot{\omega}_{x'}\rho_{cz'} \tag{20}$$

$$\dot{\omega}_{x'} = (A_{0y'} - A_{cy'})/\rho_{cz'} + \omega_{y'}\omega_{z'} \tag{21}$$

By eliminating the angular velocity terms in Equations (10)-(21), the angular acceleration with respect to the body-fixed coordinate system for the NAP scheme can be calculated using the following algebraic equations (Padgaonkar et al., 1975):

$$\dot{\omega}_{x'} = (A_{0y'} - A_{cy'})/2\rho_{cz'} - (A_{0z'} - A_{bz'})/2\rho_{by'} \tag{22}$$

$$\dot{\omega}_{y'} = (A_{0z'} - A_{az'})/2\rho_{ax'} - (A_{0x'} - A_{cx'})/2\rho_{cz'} \tag{23}$$

$$\dot{\omega}_{z'} = (A_{0x'} - A_{bx'})/2\rho_{by'} - (A_{0y'} - A_{ay'})/2\rho_{ax'} \tag{24}$$

It is important to note that any of Equations (12), (13), (15), (17), (19), and (21) can yield angular accelerations with respect to the body-fixed coordinate system directly if the angular velocity is measured using angular rate sensors. Figure 2(b) illustrates the 6aω scheme utilized in this study, where one of the accelerometers at each point is substituted with an angular rate sensor. In this configuration, Equations (12),

(17) and (21) can be used to calculate the angular accelerations algebraically. If the angular rate sensors in Figure 2(b) were substituted for $A_{az'}$, $A_{bx'}$, and $A_{cy'}$ instead of $A_{ay'}$, $A_{bz'}$, and $A_{cx'}$, then Equations (13), (15), and (19) would be used to determine the angular accelerations. With regard to angular velocity, in the NAP scheme Equations (22)-(24) must be numerically integrated, whereas in the 6aω scheme the angular velocity is directly measured by the angular rate sensors.

A 3aω scheme (three accelerometers and three angular rate sensors) can also be used to measure 3-D head kinematics. In this scheme the angular velocity is directly measured as in the 6aω scheme, but the angular acceleration can only be determined by numerically differentiating the data from the angular rate sensors, which results in noisy angular accelerations. Moreover, since angular rate sensor data often contains quite a bit of inherent noise (Martin et al., 1998), the numerical differentiation effect is amplified. In this study, the 3aω scheme was evaluated using the three accelerometers at the point of origin and the angular rate sensor at each point shown in Figure 2(b) for comparison with the data from the 6aω and NAP schemes.

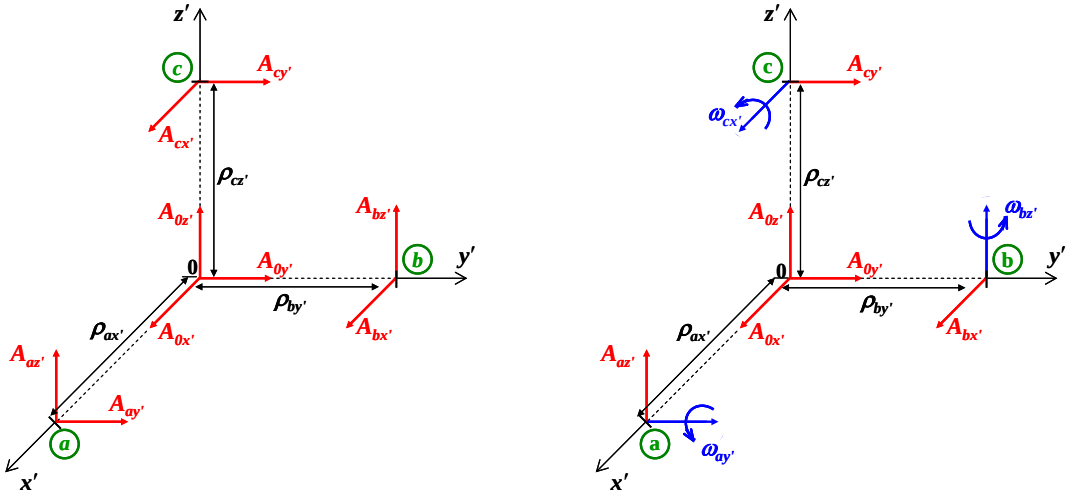

a. NAP scheme b. 6aω scheme

Figure 2: Head instrumentation configurations

Table 1 details the numerical advantages and disadvantages for all three schemes when calculating the 3-D head kinematics at an inaccessible point, such as the head CG, in the body-fixed coordinate system. The angular acceleration can be determined using algebraic equations for both the 6aω scheme (Equations (12), (17), and (21)) and the NAP scheme (Equations (22)-(24)), while the measured angular velocity data must be numerically differentiated in the 3aω scheme. Equation (8) is used in all three schemes to obtain the linear acceleration at the inaccessible point ($\underline{\ddot{\mathbf{r}}'^{P}}$), and it is important to note that this equation depends on four kinematic components: $\underline{\ddot{\mathbf{r}}'}$, $\underline{\tilde{\dot{\boldsymbol{\omega}}}'}$, $\underline{\tilde{\boldsymbol{\omega}}'}$, and $\underline{\mathbf{s}'^{P}}$. The linear acceleration term, $\underline{\ddot{\mathbf{r}}'}$, is measured directly from the accelerometers in all three schemes, and the position term, $\underline{\mathbf{s}'^{P}}$, between the origin of the instrumentation and the inaccessible point is determined by digitizing points on the head (i.e., bony land marks) and instrumentation fixture using a Faro arm device. Therefore if one assumes that $\underline{\ddot{\mathbf{r}}'}$ and $\underline{\mathbf{s}'^{P}}$ are sufficiently accurate since they are directly measured, the accuracy of the linear acceleration at the inaccessible point is dependent on the accuracy of the angular acceleration, $\underline{\tilde{\dot{\boldsymbol{\omega}}}'}$, and angular velocity, $\underline{\tilde{\boldsymbol{\omega}}'}$, with respect to the body-fixed coordinate system. In the 6aω scheme, $\underline{\tilde{\dot{\boldsymbol{\omega}}}'}$ is obtained from algebraic equations and $\underline{\tilde{\boldsymbol{\omega}}'}$ is directly measured from the angular rate sensors so it has numerical advantages over the NAP and 3aω schemes where numerical integration and/or numerical differentiation are required as shown in Table 1. Angular velocity with respect to the body-fixed coordinate system is directly measured from the

angular rate sensors in both the 6aω and 3aω schemes, while numerical integration of angular acceleration is required in the NAP scheme. This provides a numerical advantage for the 6aω and 3aω schemes over the NAP scheme, not only for angular velocity but also for linear velocity at an inaccessible point, also shown in Table 1. In summary, Table 1 shows that there is numerical evidence that the 6aω scheme should theoretically provide more accurate 3-D kinematics of the head than both the 3aω and the NAP schemes.

Additional numerical advantages and disadvantages for the three schemes are illustrated in Table 2 for measuring 3-D kinematics of the head in the global coordinate system, and again the 6aω scheme demonstrates numerical advantage theoretically over both the 3aω and the NAP schemes. It should be noted that the transformation matrix, **A**, which is a time-dependent function of the Euler angles, plays an important role in determining the global kinematics (Table 2). The accuracy of the transformation matrix at each point in time depends on the accuracy of the angular velocity in the body-fixed coordinate system. Thus, the 6aω scheme should have a more accurate transformation matrix than the NAP scheme, due to single numerical integration to yield the updated Euler angles rather than double numerical integration.

Table 1. Comparison of 6aω with 3aω and NAP : 3-D kinematics at an inaccessible point in the body-fixed coordinate system (numerical advantages shown in bold)

		NAP	3aω	6aω
Acceleration	Linear → $\underline{\ddot{r}'}$	$\underline{\tilde{\omega}'}$:Single numerical integration	$\underline{\tilde{\dot{\omega}}'}$:Numerical differentiation	**Algebraic equations**
	Angular → $\underline{\tilde{\dot{\omega}}'}$	**Algebraic equations**	Numerical differentiation	**Algebraic equations**
Velocity	Linear → $\underline{\dot{r}'}$	$\underline{\dot{r}'}$, $\underline{\tilde{\omega}'}$:Single numerical integration	$\underline{\dot{r}'}$ **:Single numerical integration**	$\underline{\dot{r}'}$ **:Single numerical integration**
	Angular → $\underline{\tilde{\omega}'}$	Single numerical integration	**Direct measurement**	**Direct measurement**

Table 2. Comparison of 6aω with 3aω and NAP: 3-D kinematics at an inaccessible point in the global coordinate system (numerical advantages shown in bold)

	NAP	3aω□	6aω
Transformation matrix → **A**	Double numerical integration	**Single numerical integration**	**Single numerical integration**
Acceleration → $\underline{\ddot{\mathbf{r}}}^{\mathbf{P}}$	- **A**: Double numerical integration - $\underline{\tilde{\omega}'}$:Single numerical integration **-** $\underline{\tilde{\dot{\omega}}'}$ **:Algebraic equations**	**- A: Single numerical integration** **-** $\underline{\tilde{\omega}'}$ **: Direct measurement** - $\underline{\tilde{\dot{\omega}}'}$:Numerical Differentiation	**- A: Single numerical integration** **-** $\underline{\tilde{\omega}'}$ **: Direct measurement** **-** $\underline{\tilde{\dot{\omega}}'}$ **:Algebraic equations**
Velocity → $\underline{\dot{\mathbf{r}}}^{\mathbf{P}}$	- **A**: Double numerical integration **-** $\underline{\dot{r}}$ **: Single numerical integration** - $\underline{\tilde{\omega}'}$:Single numerical integration	**- A: Single numerical integration** **-** $\underline{\dot{r}}$ **: Single numerical integration** **-** $\underline{\tilde{\omega}'}$ **: Direct measurement**	**- A: Single numerical integration** **-** $\underline{\dot{r}}$ **: Single numerical integration** **-** $\underline{\tilde{\omega}'}$ **: Direct measurement**

Displacement → $\underline{\mathbf{r}}^{P}$	- **$\underline{A}$**: Double numerical integration - $\underline{r}$: Double numerical integration	**- $\underline{A}$: Single numerical integration** - $\underline{r}$: Double numerical integration	**- $\underline{A}$: Single numerical integration** - $\underline{r}$: Double numerical integration

Head impact test

Two head impact tests were conducted using a Hybrid III head equipped with an internal nine-accelerometer array package (i.e., Hybrid III NAP head), along with an additional three internal angular rate sensors. The overall goal of these head impact tests was to compare the kinematics of the Hybrid III head subjected to a three-dimensional impact condition using an internal version of each of the three instrumentation schemes evaluated in this study (iNAP, i6aω, i3aω, where "i" stands for internal). Since iNAP is a well-established methodology for calculating the 3-D kinematics of the head CG of an ATD (particularly linear and angular accelerations), the first objective in the head impact tests was to compare the angular accelerations obtained using the i6aω and i3aω schemes to the angular accelerations obtained using the iNAP scheme. In addition, since it is often required to transform the head kinematics from the point of measurement to a different point on the head, the second objective in the head impact tests was to transform the iNAP, i6aω, and i3aω accelerations from the head CG to two external points on the head, and compare them with the accelerations measured directly at the two external points.

The Hybrid III head was instrumented with nine accelerometers (Endevco model 7264C 2K) and three angular rate sensors (DTS ARS-12K) in the configuration shown in Figure 3(a). This configuration of sensors allowed for the three instrumentation schemes to be directly compared during the events: an internal nine accelerometer array (iNAP), three internal accelerometers and three internal angular rate sensors (i3aω), and six internal accelerometers and three internal angular rate sensors (i6aω). A list of the instrumentation employed for each scheme in these tests is provided in Table 3. Although the locations of the angular rate sensors in the i6aω scheme shown in Figure 3(a) differ from those shown in Figure 2(b), the angular rate sensors are attached to a rigid body so their location can vary as long as they measure along the axes of the body fixed coordinate system. In contrast, it is important that the relative locations and directions of the six accelerometers employed in the i6aω scheme (three at the center of gravity and three at each point a, b, c) remain as shown in Figure 2(b) in order to determine the angular acceleration with respect to the body-fixed coordinate system. Two triaxial accelerometer clusters were also attached externally to the skin of the ATD using double-sided tape and duct tape, so that accelerations measured directly from these accelerometers could be compared to accelerations from each instrumentation scheme transformed from the head CG to these locations. Two high speed video cameras recorded the event at 1000 f/s with one anterior view along the global X axis and a lateral view along the global Y axis.

The Hybrid III head was struck by a pneumatic impactor with a mass of 23.9 kg, at impact velocities of 2.3 m/s (≈ 63 J) and 4.0 m/s (≈ 191 J). In order to generate 3-D kinematics of the head, the lower neck of the Hybrid III was attached to a fixture that was rotated 45 degrees as shown in Figure 3(b) to ensure that the impactor would collide with the head postero-laterally. The body-fixed coordinate system (x'-y'-z') on the Hybrid III head and global coordinate system (X-Y-Z) were defined as shown in Figure 3. Four points on the Hybrid III head were digitized using a Faro arm device (Faro Arm Technologies, Lake Mary FL) in order to define the initial 3-D orientation of the head, and additional points were taken to define the location of the external accelerometer clusters relative to the head CG.

For all three schemes (iNAP, i6aω, i3aω), data from the accelerometers was filtered at CFC 1000 (1650 Hz) according to SAE J211 (SAE, 2007). For the i6aω and iNAP schemes where the angular acceleration was calculated using algebraic equations, data from the angular rate sensors was also filtered at CFC 1000. Since the 3aω scheme requires numerical differentiation to obtain angular acceleration, non-standard filter classes were used in this scheme for processing data from the angular rate sensors. For the low speed test the angular rate sensors were filtered at CFC 60 (100 Hz), but due to the severity of the high speed test a CFC 180 (300 Hz) filter was chosen to be the most appropriate for the angular rate sensors, for reasons that will be explained in the Discussion section.

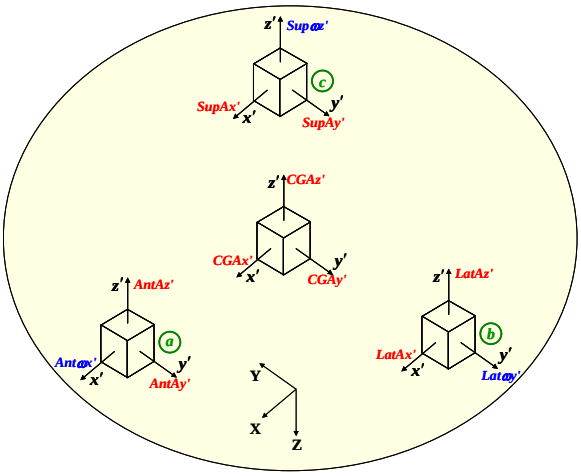

a. Instrumentation configuration (iNAP, i3aω, and i6aω)

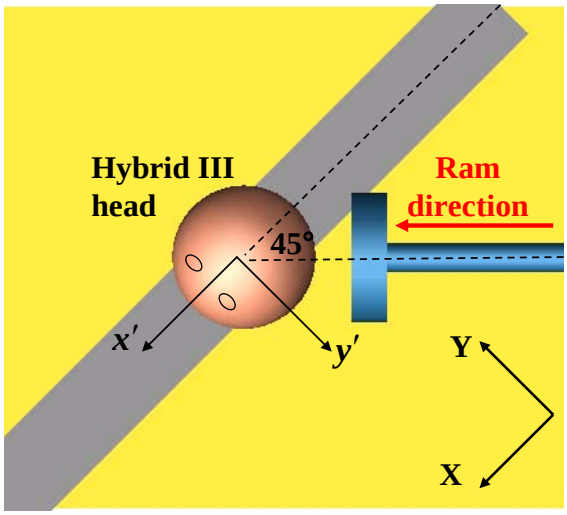

b. Test set-up and coordinate systems

Figure 3: Test set-up and instrumentation configuration

Table 3. Instrumentation employed for each scheme

	Accelerometers and angular rate sensors used from Figure 3(b)
iNAP	*CGAx', CGAy', CGAz', AntAy', AntAz', LatAx', LatAz', SupAx', SupAy'*
i3aω	*CGAx', CGAy', CGAz', Antωx', Latωy', Supωz'*
i6aω	*CGAx', CGAy', CGAz', AntAz', LatAx', SupAy', Antωx', Latωy', Supωz'*

Rear impact ATD sled test

The internal 6aω scheme utilized in the head impact tests is useful for calculating ATD head kinematics where instrumentation can be placed at the head CG and elsewhere within the Hybrid III NAP head, but for a PMHS test the sensors must be mounted on an external fixture and then transformed to the inaccessible head CG. Therefore, the primary goal in the rear impact ATD sled test was to compare the kinematics obtained using the 6aω and 3aω instrumentation scheme installed on an external fixture (and then transformed to the head CG), with the kinematics measured internally at the head CG.

An example of an external fixture which can be attached to a PMHS head is the aluminum tetrahedron utilized in Yoganandan et al. (2006) on which they installed nine accelerometers. For the current study, a similar tetrahedron fixture was used but with the 6aω instrumentation configuration (t6aω, where "t" stands for tetrahedron) installed as shown in Figure 4. The edge length of the tetrahedron is approximately 6 cm, while the mass of the fixture is only 72 grams.

A rear impact sled test (10.5g, 24 km/h) was conducted using a Hybrid III dummy with the NAP head and with the aluminum tetrahedron fixture attached to the outside of the Hybrid III head (skin removed) in the forehead region using double-sided tape and duct tape. Six accelerometers (Endevco model 7264C

2K) and three angular rate sensors (DTS ARS-12K) were installed on the aluminum tetrahedron fixture, and nine accelerometers (Endevco model 7264C 2K) were installed inside the Hybrid III head. Since the seat used in the rear impact sled tests constrained the event to a two dimensional impact condition, a single angular rate sensor was also installed at the Hybrid III head CG in the *y'* direction so that full 2-D kinematics could be measured directly at the CG for comparison with the other instrumentation schemes during the event.

Two body-fixed coordinate systems were defined, one on the tetrahedron fixture (Figure 4) and one on the Hybrid III head (Figure 5). A global coordinate system was also defined according to SAE J211 (SAE, 2007) as shown in Figure 5. For all three schemes (iNAP, t6aω and t3aω), data from the accelerometers was filtered at CFC 1000. For the t6aω and iNAP schemes the data from the angular rate sensors were also filtered at CFC 1000, and for the t3aω scheme the data from the angular rate sensors was filtered at CFC 60 and then numerically differentiated. A Faro arm device was used to define the initial 3-D orientation of the instrumentation on the tetrahedron, and its location relative to the head CG. A high speed camera mounted on the sled recorded a lateral view of the event at 1000 f/s.

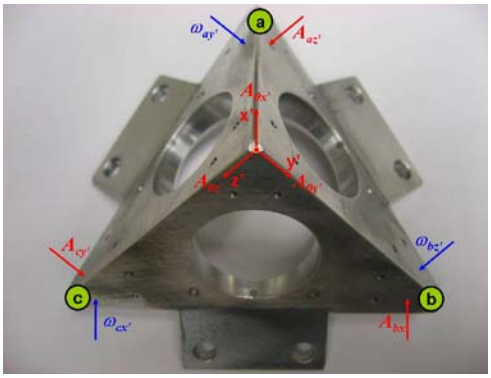

Figure 4: 6aω scheme on the aluminum tetrahedron fixture

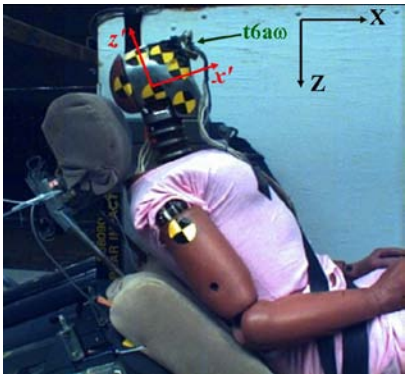

Figure 5: Test configuration and coordinate systems

Rear impact PMHS lab test

The final phase of this study was to install the tetrahedron fixture with the 6aω instrumentation scheme on the head of a PMHS subject, and validate the accuracy of the global head kinematics obtained from the instrumentation relative to the kinematics obtained from high speed video. To accomplish this, a 10 km/h rear impact lab trial was conducted using a PMHS (age: 82, weight: 72.1 kg, height: 175 cm) seated in a rigid rolling chair. The tetrahedron fixture with 6aω instrumentation installed was secured to the PMHS head using screws (Figure 6) and high speed video was recorded during the event at 1000 f/s. The global coordinate system was defined according to SAE J211 (SAE, 2007). The data from the six accelerometers and three angular rate sensors were filtered at CFC 1000.

Figure 6: 6aω scheme attached to the PMHS head

Quantitative Comparisons

In order to assess the effectiveness of the instrumentation schemes being evaluated in each test, the data obtained from each scheme was quantitatively compared to a "gold standard" chosen to be the most relevant for that comparison. The quantitative comparison was accomplished by calculating the mean square error (MSE) over time between the instrumentation scheme being evaluated (Y_i) and the gold standard (Y'_i), as shown in Equation (25). The square root was then taken to obtain the root mean square deviation (RMSD) as in Equation (26), and then the RMSD was divided by the range of the gold standard (Y'_{max} - Y'_{min}) to obtain the normalized root mean squared deviation (NRMSD), as shown in Equation (27). The NRMSD effectively provides an average percent error over time between the kinematic data obtained from the instrumentation scheme being evaluated and the gold standard.

$$MSE = \frac{\sum_{i=0}^{n}(Y_i - Y_i')^2}{n} \tag{25}$$

$$RMSD = \sqrt{\frac{\sum_{i=0}^{n}(Y_i - Y_i')^2}{n}} \tag{26}$$

$$NRMSD = \frac{RMDS}{Y'_{\max} - Y'_{\min}} \tag{27}$$

where: Y_i and Y'_i are the ith data point obtained from the instrumentation scheme being evaluated and the ith data point obtained from the gold standard, respectively.

n is the total number of data points

Y'_{max} and Y'_{min} represent the maximum and minimum values of the gold standard.

RESULTS

Head impact test

In the head impact tests three internal schemes were compared and evaluated: an internal nine accelerometer array (iNAP), six internal accelerometers with three internal angular rate sensors (i6aω), and three internal accelerometers with three internal angular rate sensors (i3aω). The first objective in the head impact test was to compare the angular accelerations obtained using the i6aω and i3aω schemes to the angular accelerations obtained using the iNAP scheme. The second objective was to transform the iNAP, i6aω, and i3aω accelerations from the head CG to two external points on the head, and compare them with the accelerations measured directly at the two external points.

For the first head impact test objective the angular accelerations obtained from the i6aω and i3aω schemes were each quantitatively compared to the angular accelerations obtained from the iNAP scheme, which was chosen as the gold standard in this comparison because it is a well-established methodology for calculating the 3-D kinematics of the ATD head CG. Figures 7 and 8 show the angular acceleration about each axis of the body-fixed coordinate system as well as the resultant, for each scheme in both the low and high speed head impact tests. Qualitative evaluation of the curves shown in Figures 7 and 8 reveal good agreement between the proposed 6aω scheme and the NAP scheme, while the 3aω method seems to be inaccurate in the high speed impact test due to noise from numerical differentiation (see Discussion section). To quantify this, NRMSD values of the angular acceleration between the gold standard iNAP scheme (Y'_i) and the i6aω and i3aω schemes (Y_i) were calculated over the first 100 ms for the low speed impact and the first 30 ms for the high speed impact. The NRMSD values presented in Figures 7 and 8 provide evidence that the i6aω scheme is capable of measuring accurate angular accelerations of the head, with less than 2% error between the i6aω and the iNAP scheme even for the high speed test. There was less than 4% error between the i3aω and iNAP schemes for the low speed test, but the error increased to values between 9% and 16% in the high speed test. The larger errors reveal that the i3aω scheme may not be appropriate to measure 3-D head angular accelerations during severe head impact conditions, due to excessive noise from the numerical differentiation in the i3aω scheme.

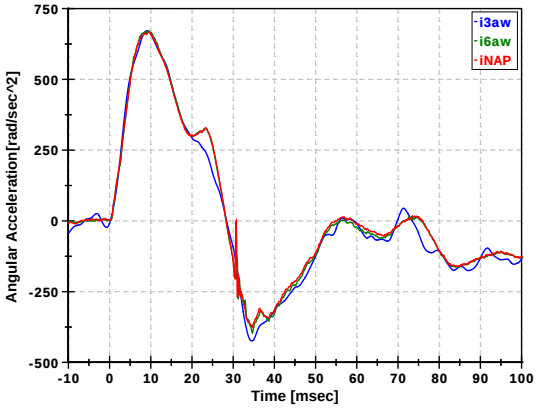

a. Angular acceleration in the *x'* axis
i6aω vs. iNAP: NRMSD = 1.20 %
i3aω vs. iNAP: NRMSD = 3.02 %

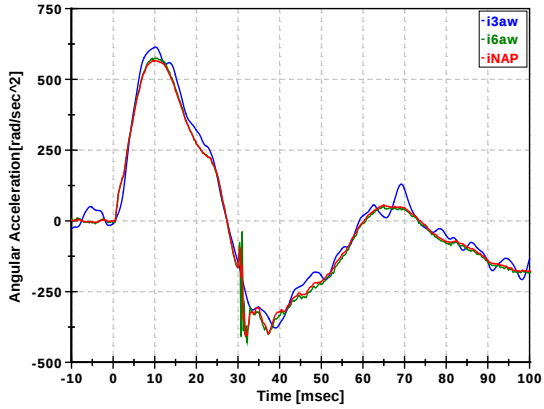

b. Angular acceleration in the *y'* axis
i6aω vs. iNAP: NRMSD = 1.33 %
i3aω vs. iNAP: NRMSD = 3.41 %

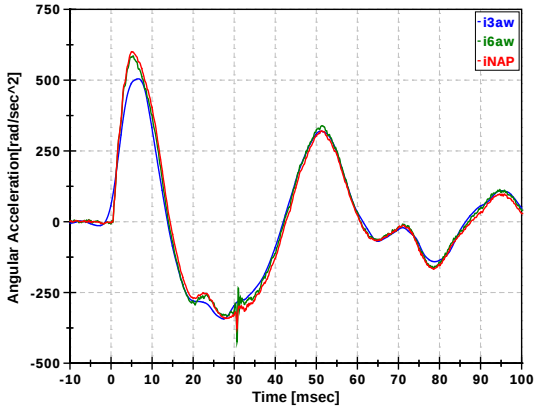

c. Angular acceleration in the z' axis
i6aω vs. iNAP: NRMSD = 1.59 %
i3aω vs. iNAP: NRMSD = 3.36 %

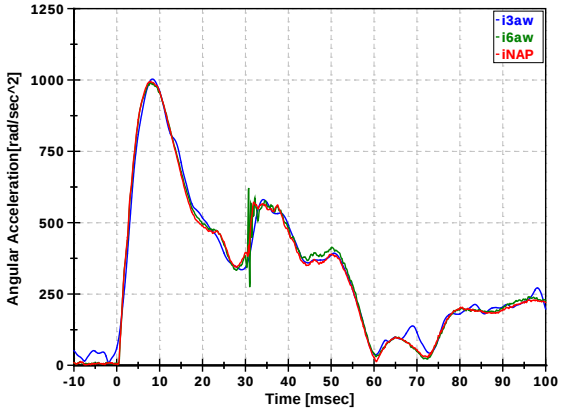

d. Resultant of angular acceleration
i6aω vs. iNAP: NRMSD = 1.57 %
i3aω vs. iNAP: NRMSD = 2.80 %

Figure 7: Comparison of angular acceleration (i6aω vs. iNAP, i3aω vs. iNAP)
Low-speed head impact test (2.3 m/s)

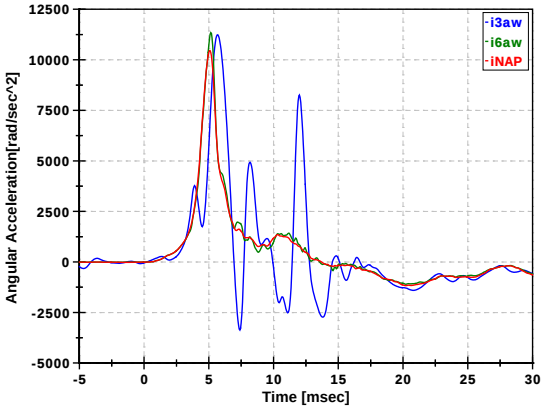

a. Angular acceleration in the x' axis
i6aω vs. iNAP: NRMSD = 1.25 %
i3aω vs. iNAP: NRMSD = 16.30 %

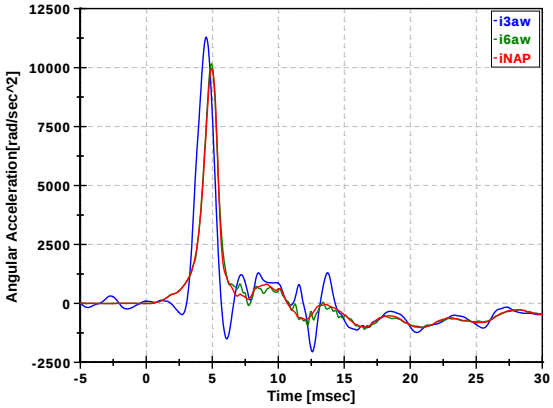

b. Angular acceleration in the y' axis
i6aω vs. iNAP: NRMSD = 1.04 %
i3aω vs. iNAP: NRMSD = 9.46 %

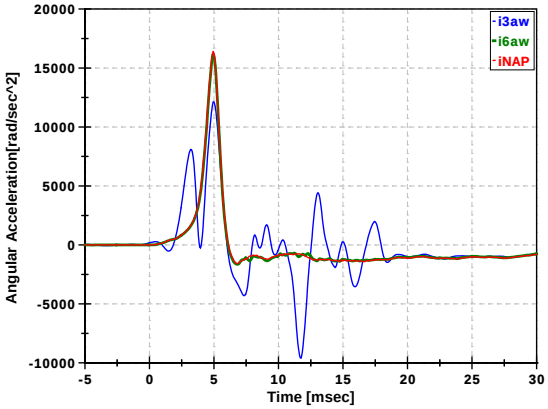

c. Angular acceleration in the z' axis
i6aω vs. iNAP: NRMSD = 0.44 %

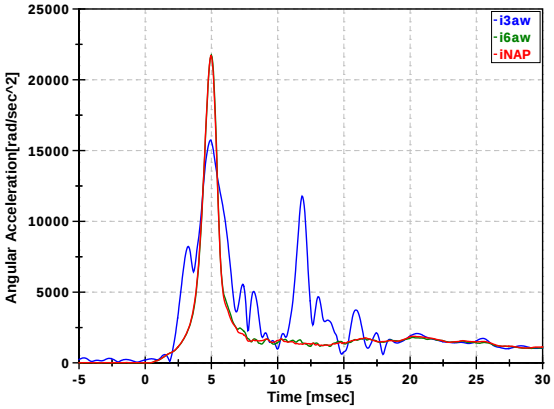

d. Resultant of angular acceleration
i6aω vs. iNAP: NRMSD = 0.46 %

i3aω vs. iNAP: NRMSD = 11.60 % i3aω vs. iNAP: NRMSD = 10.24 %

Figure 8: Comparison of angular acceleration (i6aω vs. iNAP, i3aω vs. iNAP)
High-speed head impact test (4.0 m/s)

It is important in PMHS testing to be able to transform kinematic data from the peripheral head instrumentation to an inaccessible point (e.g., head CG) with respect to the body-fixed coordinate system. Therefore, for the second head impact test objective two triaxial accelerometer clusters were installed on the external surface of the Hybrid III head to simulate this effort and demonstrate the proposed transformation procedure previously shown in Equation (9). The accelerations calculated from each internal scheme at the head CG were transformed to the local coordinates of each peripheral cluster, and the resultant of the transformed internal accelerations was compared to the resultant acceleration directly measured from the peripheral sensors (Figures 9 and 10). NRMSD values were calculated between the resultant acceleration obtained from each of the i6aω, i3aω, and iNAP schemes and the resultant acceleration measured by the peripheral sensors (gold standard), and Figure 9 shows that NRMSD valued for all three schemes were less than 2% for the low speed test. The i6aω and the iNAP resultant acceleration agreed well with the measured acceleration in the high speed test (less than 3% error), but the i3aω resultant acceleration differed from the measured acceleration. This result is not surprising when Equation (9) is examined because the transformed linear acceleration, $\ddot{\underline{\mathbf{r}}}'^{b}$, is dependent on the angular acceleration, $\tilde{\underline{\dot{\boldsymbol{\omega}}}}'$, which in the 3aω scheme was shown to be inaccurate in the high speed test due to numerical differentiation (Figure 8).

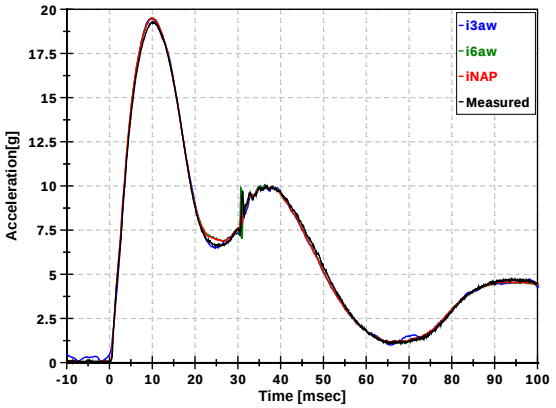

a. Resultant linear acceleration (peripheral cluster 1)
i6aω vs. measured: NRMSD = 1.12%
i3aω vs. measured: NRMSD = 1.08%
iNAP vs. measured: NRMSD = 0.98%

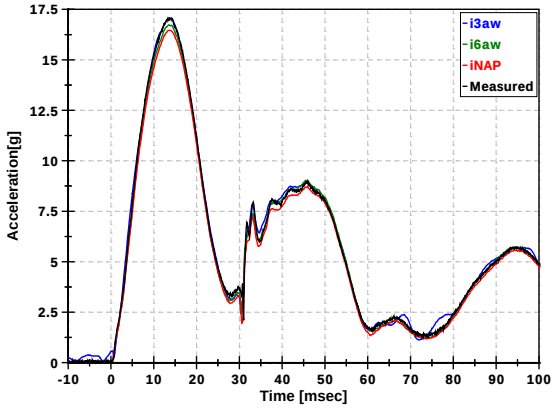

b. Resultant linear acceleration (peripheral cluster 2)
i6aω vs. measured: NRMSD = 1.13%
i3aω vs. measured: NRMSD = 1.34%
iNAP vs. measured: NRMSD = 1.79%

Figure 9: Comparison of resultant linear acceleration at peripheral clusters
(transformed i6aω, iNAP and i3aω vs. measured)
Low-speed head impact test (2.3 m/s)

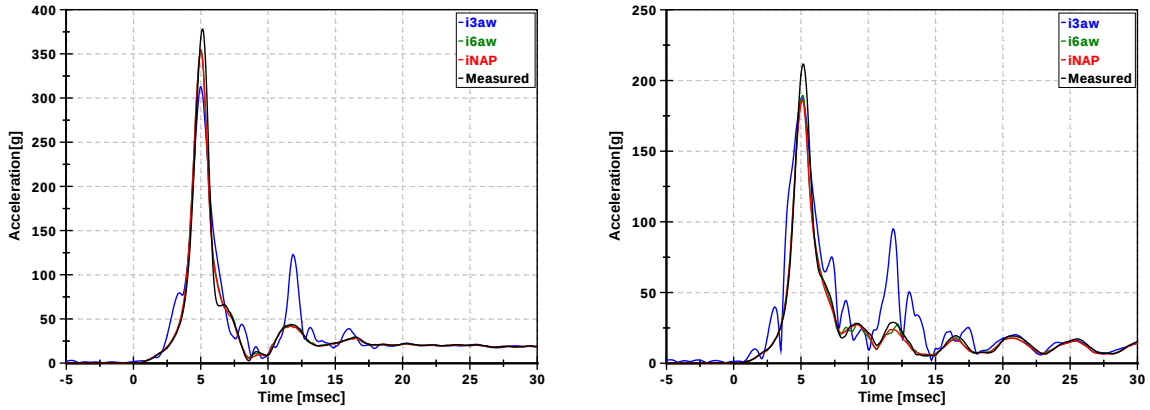

a. Resultant linear acceleration (peripheral cluster 1)
i6aω vs. measured: NRMSD = 1.97%
i3aω vs. measured: NRMSD = 4.65%
iNAP vs. measured: NRMSD = 2.30%

b. Resultant linear acceleration (peripheral cluster 2)
i6aω vs. measured: NRMSD = 2.13%
i3aω vs. measured: NRMSD = 7.32%
iNAP vs. measured: NRMSD = 2.32%

Figure 10: Comparison of resultant linear acceleration at peripheral clusters
(transformed i6aω, iNAP and i3aω vs. measured)
High-speed head impact test (4.0 m/s)

Even though the NRMSD values for the transformed i6aω and iNAP accelerations in the high speed impact test were below 3%, there was a consistent trend of potential concern in that the maximum accelerations measured at the peripheral clusters were greater than the maximum accelerations transformed from each internal instrumentation scheme (Figure 10). One possible cause for this is that the double- sided tape and duct tape did not sufficiently secure the triaxial accelerometer clusters to the skin of the Hybrid III head for the high speed impact tests (i.e., the peripheral clusters were effectively not attached to the same rigid body as the internal sensors). To investigate whether this error was indeed an attachment issue between the skin and the peripheral instrumentation the accelerations calculated from the i6aω and i3aω schemes at the head CG were transformed to three different accelerometer locations inside the Hybrid III NAP head (*AntAy'*, *LatAz'*, and *SupAx'* in Figure 3(b)). This allowed for a similar comparison as with the peripheral clusters except in this case the accelerometers at the alternate locations were rigidly attached to the head on internal mounts. It should be noted that these accelerometers were used in the angular acceleration calculation in the iNAP scheme, but not in the i6aω and i3aω schemes, so only the i6aω and i3aω schemes were evaluated at these locations. The results of this exercise are shown in Figure 11, and NRMSD values between the acceleration transformed from the i6aw scheme and the acceleration measured directly at each internal location were less than 2% for all three accelerometers, and the trend that had been observed with the maximum values for the externally mounted clusters did not appear. This provides evidence that the trend for the maximum values observed in Figure 10 may have indeed been a result of the peripheral clusters not being secured well enough for the high speed test. Figure 11 also shows that similar to the previous comparisons, the i3aω scheme performed adequately in the low speed impact test but poorly in the high speed impact test.

To summarize the results from the head impact tests, the proposed 6aω instrumentation scheme and associated mathematical analysis are capable of producing angular accelerations and linear accelerations transformed to a remote location that are comparable to the NAP instrumentation scheme in both low and high speed impact conditions. The 3aω instrumentation scheme was found to be unable to provide accurate angular accelerations during severe head impact conditions due to the required numerical differentiation. As

a result the 3aω instrumentation scheme was also unable to provide accurate linear acceleration at a remote location due to the dependency of the transformation on the angular acceleration (Equation 9).

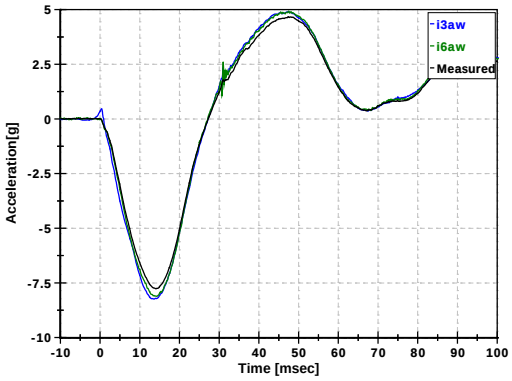

a. Linear acceleration ($A_{ay'}$)
Low speed impact (2.3 m/s)
i6aω vs. measured: NRMSD = 1.42%
i3aω vs. measured: NRMSD = 2.08%

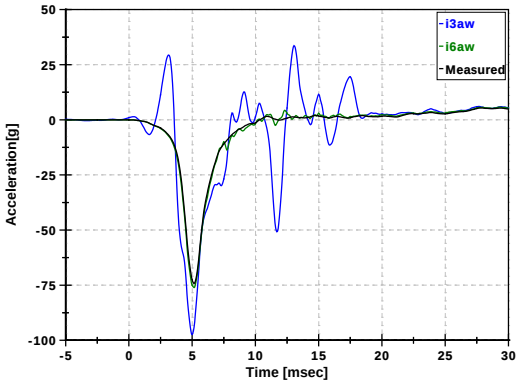

b. Linear acceleration ($A_{ay'}$)
High speed impact (4.0 m/s)
i6aω vs. measured: NRMSD = 1.13%
i3aω vs. measured: NRMSD = 15.05%

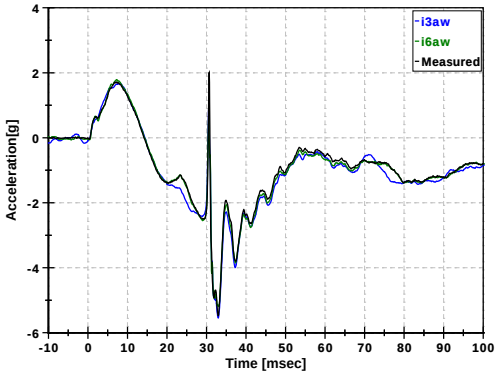

c. Linear acceleration ($A_{bz'}$)

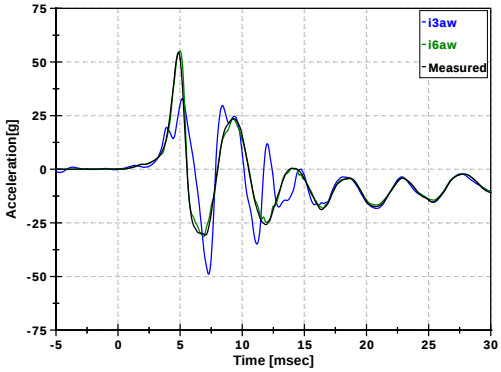

d. Linear acceleration ($A_{bz'}$)

Low speed impact (2.3 m/s)
i6aω vs. measured: NRMSD = 1.65%
i3aω vs. measured: NRMSD = 2.52%

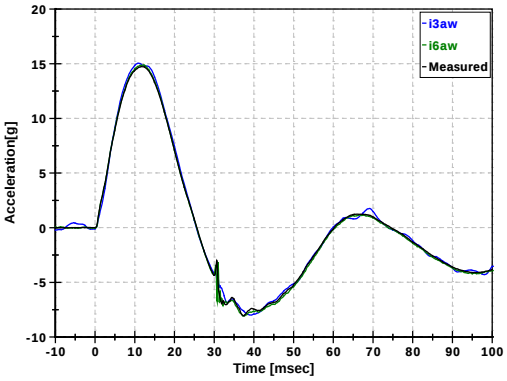

e. Linear acceleration ($A_{cx'}$)
Low speed impact (2.3 m/s)
i6aω vs. measured: NRMSD = 0.94%
i3aω vs. measured: NRMSD = 1.28%

High speed impact (4.0 m/s)
i6aω vs. measured: NRMSD = 1.67%
i3aω vs. measured: NRMSD = 10.98%

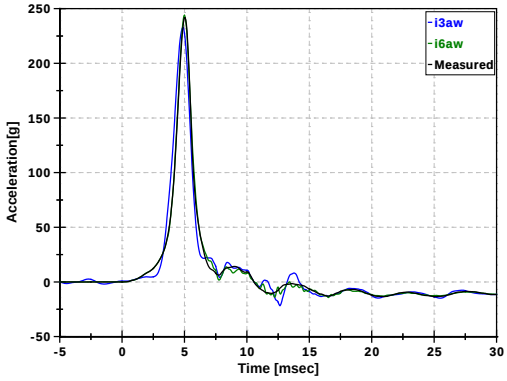

f. Linear acceleration ($A_{cx'}$)
High speed impact (4.0 m/s)
i6aω vs. measured: NRMSD = 0.74%
i3aω vs. measured: NRMSD = 3.40%

Figure 11: Comparison of linear acceleration at three internal accelerometer locations
(transformed i6aω and i3aω vs. measured)

Rear impact ATD sled test

An external fixture is generally required to measure 3-D head kinematics in PMHS testing and then the kinematics obtained at the fixture are transformed to the head CG. The goal of this test was to compare and validate the kinematics obtained using the 6aω and 3aω instrumentation scheme installed on an external tetrahedron fixture (t6aω and t3aω) with the kinematics measured internally at the head CG (iNAP).

To accomplish this, a rear impact sled test (10.5g and 24 km/h) was conducted using a Hybrid III dummy with the NAP head, and with the aluminum tetrahedron fixture attached externally. During the test, the Hybrid III head freely translated and rotated until it contacted a head restraint at approximately 104 ms. The t6aω and t3aω schemes were evaluated in comparison to the iNAP scheme which was considered the gold standard for quantitative analysis using the NRMSD (for the same reason as discussed in the head impact tests). Figure 12 shows that the NRMSD value between the t6aω and the iNAP for the angular acceleration in the primary *y'* axis as well as the resultant angular acceleration was under 2%. Although numerical differentiation in the t3aω scheme resulted in the generation of some noise in the angular acceleration, as shown in Figure 12, the results were acceptable with an NRMSD value of 2.93% in the *y'* axis and 3.81% for the resultant.

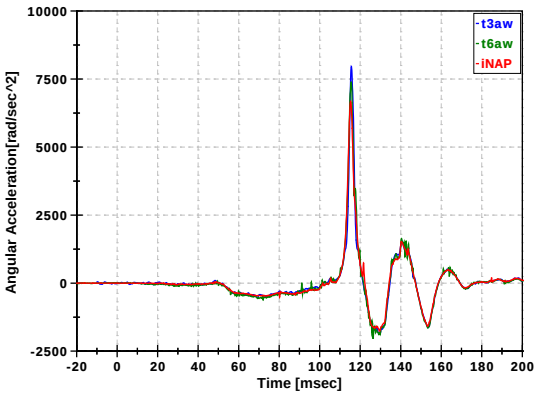

a. Angular acceleration in the *y'* axis
t6aω vs. iNAP: NRMSD = 1.58%
t3aω vs. iNAP: NRMSD = 2.93%

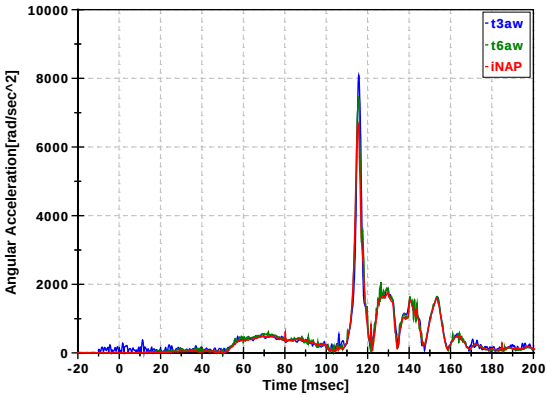

b. Resultant of angular acceleration
t6aω vs. iNAP: NRMSD = 1.99%
t3aω vs. iNAP: NRMSD = 3.81%

Figure 12: Comparison of angular acceleration (t6aω vs. iNAP, t3aω vs. iNAP)

To further evaluate the t6aω, t3aω, and iNAP schemes (similar to the second head impact test objective), the resultant acceleration data calculated from each scheme was transformed to a relevant location where the accelerations were measured directly. Specifically, the t6aω and t3aω resultant accelerations were transformed to the CG of the head to compare with the directly measured *CGAx'*, *CGAy'*, and *CGAz'* sensors used in the iNAP scheme (Figure 3). Also, the iNAP resultant acceleration was transformed to the vertex of the tetrahedron fixture to compare with the directly measured $A_{0x'}$, $A_{0y'}$, and $A_{0z'}$ sensors used in the t6aω and t3aω schemes (Figure 4). In both scenarios, the transformed resultant acceleration was quantitatively compared to the directly measured resultant acceleration (considered the gold standard for NRMSD calculations). Figure 13 shows that the transformed resultant acceleration from each scheme (i.e., t6aω/t3aω or iNAP) agreed well with the resultant acceleration measured directly at the alternate location (i.e, head CG or tetrahedron vertex), with NRMSD values less than 1% for t6aω and iNAP, and approximately 2% for t3aω.

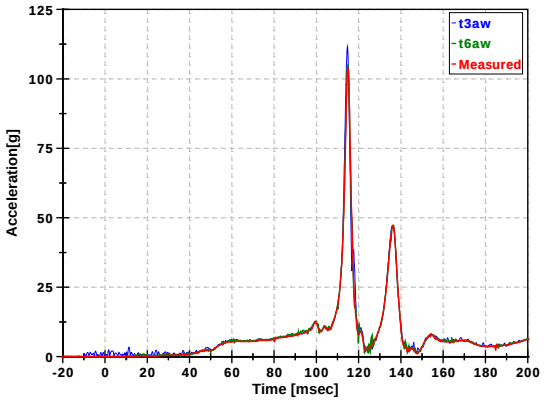

a. Resultant linear acceleration (head CG)
transformed t6aω vs. measured: NRMSD = 0.59%
transformed t3aω vs. measured: NRMSD = 2.08%

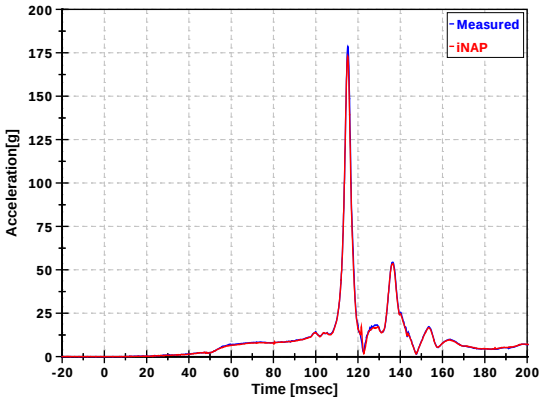

b. Resultant linear acceleration (tetrahedron vertex)
transformed iNAP vs. measured: NRMSD = 0.62%

Figure 13: Comparison of resultant linear acceleration transformed to locations of direct measurement

For the rear impact ATD sled test, the kinematics of the head CG with respect to the global coordinate system were also evaluated for the t6aω, t3aω, and iNAP schemes. Since this particular test is two dimensional, with all motion in the sagittal plane of the occupant, full 2-D kinematics of the head CG can be determined in the global coordinate system by using two accelerometers at the head CG (i.e., *CGAx'* and *CGAz'*) and an angular rate sensor at the head CG in the *y'* direction. These "measured" 2-D kinematics were considered the gold standard in this comparison. Figure 14 shows the acceleration transformed from each instrumentation scheme to the global X and Z directions previously defined in Figure 5. The NRMSD values were approximately 2% for the acceleration in both the X and Z directions, indicating that the three schemes are capable of measuring accurate global acceleration.

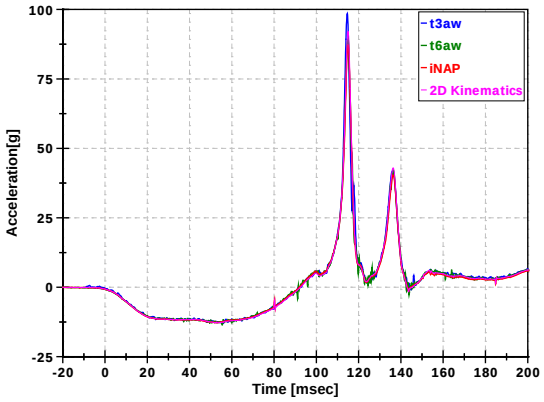

a. Linear acceleration in the global X axis
t6aω vs. 2-D kinematics: NRMSD = 0.77%
t3aω vs. 2-D kinematics: NRMSD = 2.31%
iNAP vs. 2-D kinematics: NRMSD = 0.74%

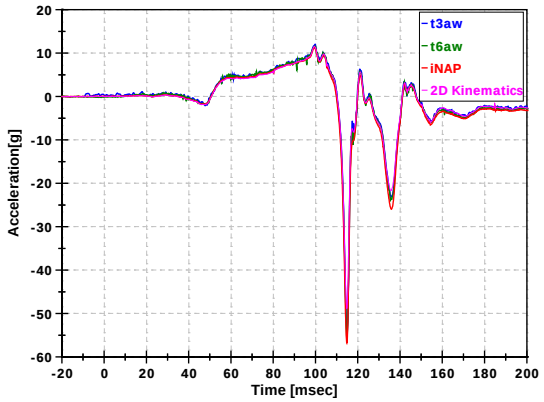

a. Linear acceleration in the global Z axis
t6aω vs. 2-D kinematics: NRMSD = 1.47%
t3aω vs. 2-D kinematics: NRMSD = 1.38%
iNAP vs. 2-D kinematics: NRMSD = 2.24%

Figure 14: Linear acceleration in the global coordinate system (X and Z)

Figure 15 shows the angular velocity and angular displacement (rotation) in the global Y axis. Global angular velocities and rotations obtained from the 3aω scheme are exactly the same as the 6aω scheme (Table 2) so the t3aω results are not displayed in Figure 15. The gold standard chosen for angular velocity was the data measured from the angular rate sensor attached to the head CG, and for rotation the gold standard was chosen to be the rotation obtained from high speed video. Even though the NRMSD values for angular velocity calculated across time were below 3% for both the t6aω and iNAP schemes, qualitative inspection of the curves reveal that the peak angular velocity obtained from the iNAP appeared to deviate from the data measured from the head CG angular rate sensor, while the data from the t6aω scheme showed consistently good agreement. With respect to rotation, the NRMSD value was 1.26% for the t6aω scheme and 4.25% for the iNAP scheme. The more accurate rotation obtained from the t6aω scheme is likely due to the double numerical integration required to obtain rotation in the iNAP scheme (Table 2). To further examine the differences between the t6aω and iNAP schemes with regard to the determination of rotation, the rotation of the head with respect to the global X and Z directions were compared (Figure 16). Since this rear impact sled test was essentially a 2-D event, these off-axis rotations should be quite small. However, while the rotation magnitudes obtained from the t6aω scheme were less than 5 degrees in both the X and Z directions, the iNAP scheme produced very large rotations (~25 degrees) in both directions. Close inspection of the video revealed that the Hybrid III head exhibited little to no rotations in the X and Z directions indicating that the 5 degrees of maximum rotation obtained from the t6aω scheme is more realistic. This provides further evidence that the proposed 6aω scheme produces more accurate rotation in the global coordinate system than the iNAP scheme.

To summarize the results from the rear impact ATD sled test, the 6aω and 3aω instrumentation schemes installed on an external tetrahedron fixture were able to produce accurate angular and linear accelerations transformed to the head CG. All three schemes (6aω, 3aω, and NAP) were able to provide accurate linear acceleration in the global coordinate system, while the 6aω and 3aω instrumentation schemes provide more accurate results for angular velocity and rotation than the NAP scheme.

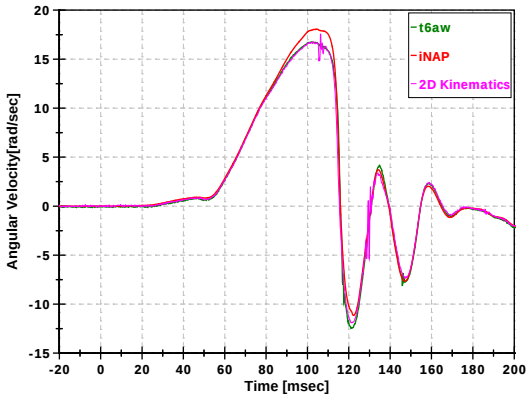

a. Angular velocity in the global Y axis
i6aω vs. 2-D kinematics: NRMSD = 2.15%
iNAP vs. 2-D kinematics: NRMSD = 2.68%

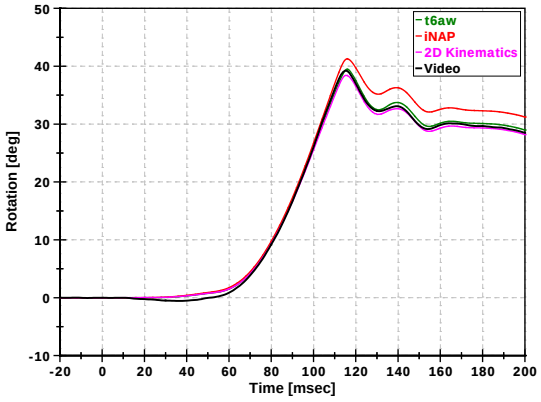

a. Rotation in the global Y axis
i6aω vs. video: NRMSD = 1.26%
iNAP vs. video: NRMSD = 4.25%

Figure 15: Angular velocity and rotation in the global coordinate system (Y)

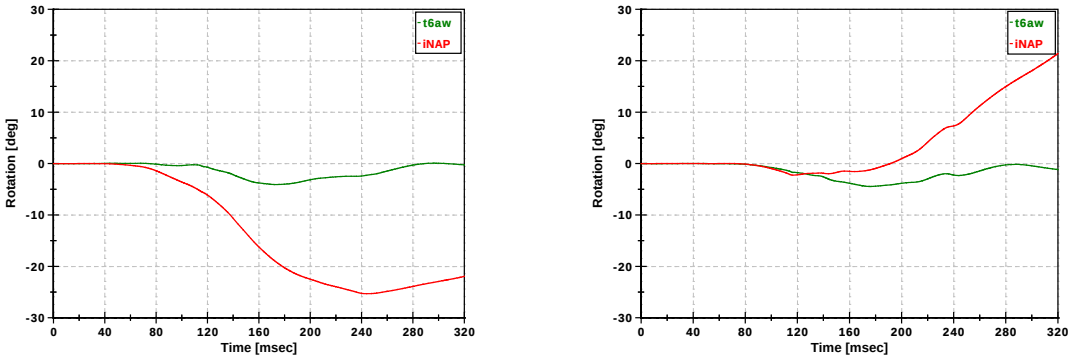

a. Rotation in the global X axis

b. Rotation in the global Z axis

Figure 16: Rotation in the global coordinate system (X and Z)

Rear impact PMHS lab test

The previous two test series indicated that the 6aω scheme installed on the tetrahedron fixture appeared to be capable of producing linear and angular accelerations comparable to the iNAP scheme, while producing more accurate angular velocity and displacement than the iNAP scheme. The final phase of this study was to further validate the 6aω scheme by conducting a PMHS test in the lab with the 6aω tetrahedron fixture installed on the head of the PMHS, and comparing the linear and angular displacement kinematics obtained from the t6aω scheme with the kinematics obtained from high speed video. The gold standard used for quantitative analysis was the kinematics obtained from the high speed video and the results are shown in Figure 17. The linear displacement data obtained from the t6aω scheme matched well over the initial 200 ms in both primary directions with NRMSD values less than 2%. After this time they began to diverge from the video analysis due to accumulation of error from the double numerical integration of the linear acceleration data. It should be noted, however, that 200 ms is typically a sufficient amount of time for data analysis in an impact event. The rotation in the primary Y direction also exhibited good agreement with the video analysis for the first 200 ms (NRMSD value of 0.57%), and even when examined to a longer duration of 360 ms (NRMSD value of 1.41%). These results provide additional evidence that the proposed 6aω scheme on the tetrahedron fixture is capable of measuring accurate displacement kinematics in the global coordinate system.

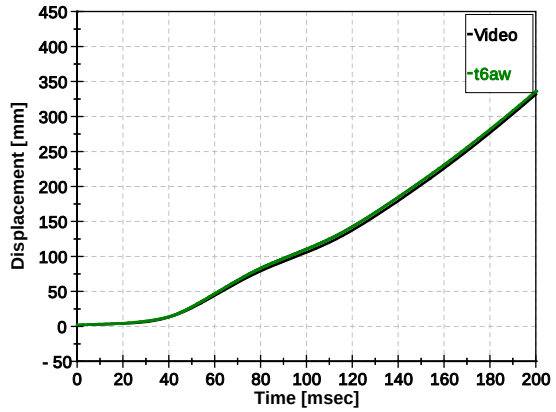

a. Displacement in the X direction
t6aw vs. video: NRMSD = 1.22 %

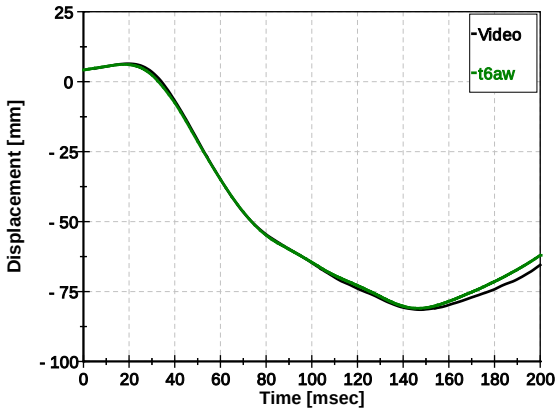

b. Displacement in the Z direction
t6aω vs. video : NRMSD = 1.55%

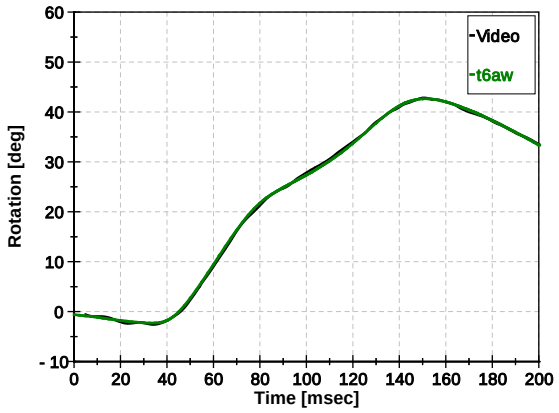

c. Rotation in the Y direction
t6aω vs. video : NRMSD = 0.57%

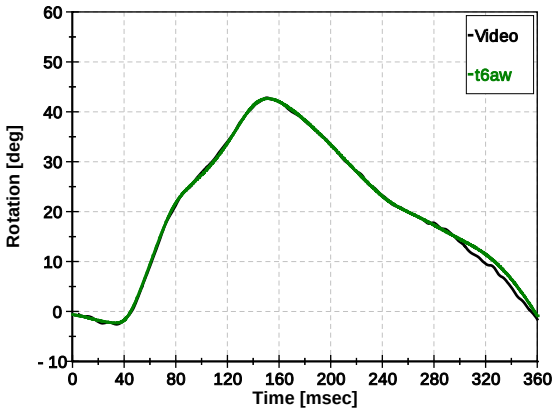

d. Rotation in the Y direction (long duration)
t6aω vs. video : NRMSD = 1.41%

Figure 17: Linear and angular displacement (rotation) of the PMHS head in the global coordinate system

DISCUSSION

Three head instrumentation schemes, the 6aω scheme, the 3aω scheme, and the NAP scheme were compared using the Hybrid III NAP head in low and high speed head impact tests, and in a rear impact sled test. Results from these tests indicated that the 6aω scheme (both internal i6aω and external t6aω) produced linear and angular accelerations as accurate as the iNAP scheme, while producing more accurate angular velocity and displacement than the iNAP scheme. This held true even in the 4.0 m/s (≈ 191 J) high severity head impact test which resulted in a peak resultant acceleration of 231.1 g (close to the threshold for injury of the skull reported by Yoganandan et al., 2006), angular acceleration of 21.7 krad/sec^2, and a HIC of 656.2.

Unlike the peripheral scheme developed by Martin et al. (1998), alignment of the 6aω instrumentation along the body fixed coordinate system is not necessary. The proposed method using the tetrahedron fixture allows for the angular acceleration of the head to be determined using algebraic equations (Equations (11), (17), and (21)), and then the linear acceleration at the head CG can be obtained using Equation (9). Results from the head impact tests and rear impact sled test show that the 6aω kinematics transformed to a location where kinematics are directly measured agree very well with the measured data (Figures 9, 10, 11 and 13). These results illustrate the capability of the 6aω method on the tetrahedron fixture to obtain accurate 3-D head kinematics.

Different filtering techniques for head instrumentation have been suggested to reduce unexpectedly high vibrations in various testing conditions (Martin et al., 1997; Martin et al., 1998; Yoganandan et al., 2006; Hardy et al., 2001; Hardy et al., 2007). For the NAP scheme, a 180 Hz filter class was used to reduce resonance of the PMHS head in a head injury study (Hardy et al., 2001), while data from the NAP scheme on the tetrahedron attached to a PMHS and Hybrid III head was filtered at 1650 Hz in Yoganandan's head drop tests (Yoganandan et al., 2006). Dynacube data (same as the 3aω scheme) was filtered at 600 Hz in a torsional pendulum test (Martin et al., 1997), while the accelerometer data and angular rate sensor data were filtered at 600 Hz and 300 Hz, respectively, in Hybrid III head drop tests (Martin et al., 1998). In contrast to these previous studies, data measured from both the accelerometers and the angular rate sensors for the 6aω scheme in this study was filtered at CFC 1000 according to SAEJ211 (SAE, 2007). Based on the results from the head impact tests and the rear impact sled test, the filtering class used in this study for both the accelerometers and angular rate sensors appears to be capable of generating accurate head kinematics without any vibration-related issues. However, in the 3aω scheme where angular acceleration is obtained by numerically differentiating the angular rate sensors, two different types of filtering classes were used for the angular rate sensors (CFC 60 for the low severity head impact test and rear impact sled test; CFC 180 for the high severity head impact test). In the low speed tests incorporating the CFC 60 filter, the kinematic data from the 3aω scheme was comparable to the data from the NAP and the 6aω schemes, but implementing CFC 60 in the high severity impact caused a large reduction in the peak angular acceleration, resulting in 66% error between the 3aω scheme and iNAP. Figure 18 reveals that regardless of the filter used, the angular acceleration from the 3aω scheme does not match that from the NAP and 6aω schemes, either due to excessive noise or excessive reduction in magnitude. Consequently, the 3aω scheme should be limited to low severity impact tests due to excessive noise produced by numerically differentiating the data measured from the angular rate sensors. In the analysis of the 3aω scheme for the high severity head impact test the CFC 180 filter was chosen because it produced results that represented the middle ground between excessive noise and excessive reduction in magnitude.

In the rear impact ATD sled test the angular and linear accelerations, angular velocity, and rotation for each instrumentation scheme with respect to the global coordinate system were evaluated (Figures 14, 15, and 16). Both the qualitative and quantitative analysis indicated that the 6aω scheme on the tetrahedron is capable of measuring the most accurate global kinematics among all three schemes. This provides experimental support for the theoretical evidence discussed in Tables 1 and 2 that the 6aω scheme should produce the most accurate kinematics, primarily because the angular velocity is directly measured rather than being determined by numerically integrating the angular acceleration. Furthermore, the transformation matrix which is a time-dependent function of the Euler angles, plays an important role in determining the global kinematics (Table 2). To obtain the transformation matrix, the first time derivative of the Euler angle terms is determined algebraically as a function of the angular velocity with respect to the body-fixed

coordinate system, and then the Euler angles at each point in time can be found by numerically integrating these terms. Therefore, the accuracy of the transformation matrix at each point in time depends on how accurate the angular velocity in the body-fixed coordinate system can be determined, thus the 6aω scheme should have a more accurate transformation matrix than the NAP, due to single numerical integration instead of double numerical integration.

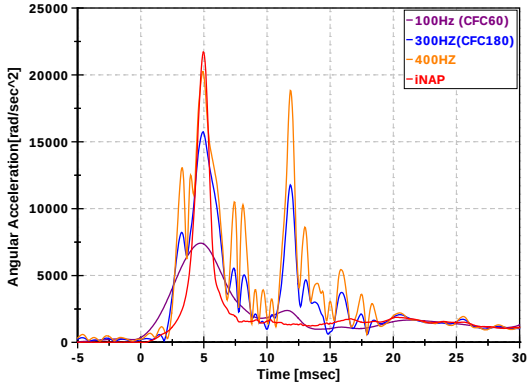

Fig. 18 Resultant angular acceleration for the iNAP vs. the 3aω scheme using different filtering classes

A final illustration of how the various strengths of the 6aω scheme discussed in Tables 1 and 2 can significantly reduce the error in the measurement of global rotations is shown in Figure 19. The rotation of the head in the high speed impact test determined using the i6aω scheme and the iNAP scheme is shown in the global X and Y directions relative to the rotation determined from high speed video (gold standard). The rotation determined from the 6aω scheme matches the high speed video very well over the entire 500 ms (NRMSD values of 0.92% and 2.70%), while the rotation determined from the iNAP scheme begins to deviate from the high speed video around 70 ms due to the errors that accumulate from double numerical integration. These results support the findings from Nusholtz (1993) where hypothetical examples were used to compare angular displacement from a nine accelerometer 3-3-3 array to that from a 3-2-2-2 array.

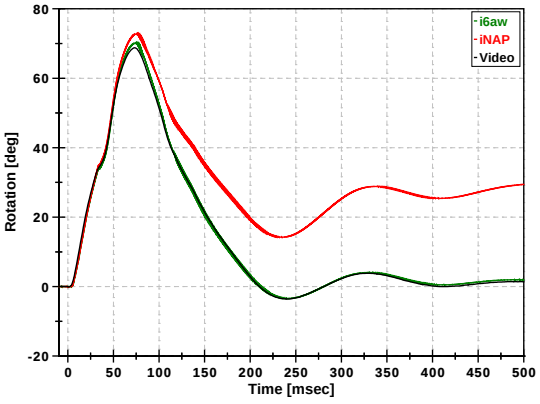

a. Rotation in the X direction
i6aω vs. video: NRMSD = 0.92 %
iNAP vs. video: NRMSD = 27.95 %

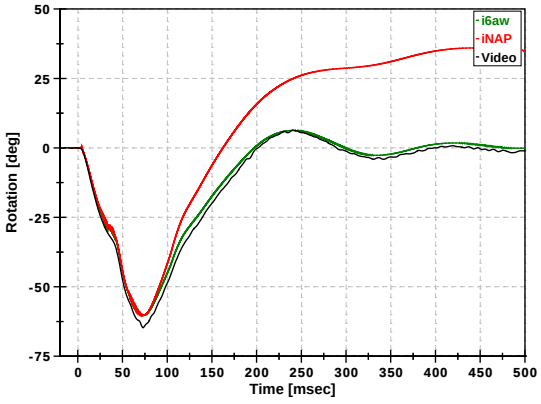

b. Rotation in the Y direction
i6aω vs. video: NRMSD = 2.70 %
iNAP vs. video: NRMSD = 33.95 %

Fig. 19 Angular displacement comparison in the high speed head impact test

CONCLUSIONS

In this study, an improved instrumentation technique to measure 3-D head kinematics employing six accelerometers and three angular rate sensors (6aω) was proposed and validated on both a Hybrid III NAP head and a PMHS head. The 6aω scheme was validated by conducting low and high speed head impact tests (2.3 m/s and 4.0 m/s), a 10.5 g, 24 km/h rear impact sled test with a Hybrid III dummy with the NAP head, and a 10 km/h rear impact test with a PMHS in a rigid rolling chair. Initial 3-D orientation of each scheme (NAP, 6aω, and 3aω) was defined by digitizing points on either a tetrahedron fixture or the Hybrid III head. Data from each scheme was transformed to either the center of gravity or to various locations where redundant accelerometers were installed, and quantitative comparisons using the NRMSD were made between each scheme being evaluated and the relevant gold standard. The advantages of the proposed 6aω scheme are the ability to use an algebraic equation to determine angular acceleration and to directly measure angular velocity instead of relying on numerical integration of the angular acceleration. The proposed method provides accurate kinematics in the body-fixed and global coordinate systems as well as an accurate transformation matrix determined at each point in time. The proposed 6aω scheme on the tetrahedron fixture appears to be capable of measuring accurate 3-D kinematics of the head, and will allow for PMHS to be tested in any severity of impact conditions. The kinematic data obtained from the 6aω scheme in future testing should aid in the development and evaluation of injury criteria in studies involving the head and neck.

ACKNOWLEDGEMENTS

This research was completed under DOT/NHTSA contract (DTNH22-08-D-00082).

REFERENCES

BECKER, E., and WILLEMS, G., (1975). "An experimentally validated 3-D inertial tracking package for application in biodynamic research," J. Stapp Car Crash, 19, SAE Paper 751173.

BENDJELLAL, F., OUDENARD, L., URIOT, J., BRIGOUT, C., and BRUN-CANAU, F., (1990). "Computation of hybrid III head dynamics in various impact situations," J. Stapp Car Crash, 34, SAE Paper 902320.

BENDJELLAL, F., OUDENARD, L., ELLER, E., KOCH, M., PLANATH, I., and TARRIERE, C., (1992). "Measurement of head angular acceleration in crash tests: development of an electronic device for the hybrid III dummy," J. Stapp Car Crash, 36, SAE Paper 922511

DENG, B., BEGEMAN, P. C., YANG, K. H., TASHMAN, S., and KING, A. I., (2000). "Kinematics of Human Cadaver Cervical Spine During Low Speed Rear-end Impacts," J. Stapp Car Crash, 44, SAE Paper No. 2000-01-SC13.

DIMASI, F.P., EPPINGER. R.H., and BANDAK, F.A., (1995). "Computational Analysis of Head Impact Response Under Car Crash Loadings," J. Stapp Car Crash, 39, SAE Paper 952718.

DIMASI, F.P., (1995). "Transformation of Nine-Accelerometer-Package (NAP) Data for Replicating Headpart Kinematics and Dynamic Loading," NHTSA Technical Report, DOT HS 808 282.

EWING, C.L., THOMAS, D.J., MAJEWSKI, P.L., BLACK, R., and LUSTICK, L., (1977a). "Measurement of head, T1, and pelvic response to -Gx impact acceleration," J. Stapp Car Crash, 21, SAE Paper 770927.

EWING, C.L., THOMAS, D.J., LUSTICK, L., MUZZY, W.H., WILLEMS, G.C., and MAJEWSKI, P., (1977b). "Dynamic response of the human head and neck to +Gy impact acceleration," J. Stapp Car Crash, 21, SAE Paper 770928.

EWING, C.L., THOMAS, D.J., LUSTICK, L., BECKER, E., WILLEMS, G.C., and MUZZY, W.H., (1975). "The effect of the initial position of the head and neck on the dynamic response of the human head and neck to -Gx impact acceleration," J. Stapp Car Crash, 19, SAE Paper 751157.

HARDY, W.N., MASON, M., FOSTER, C.D., SHAH, C.S., KOPACZ, J.M., YANG, K.H., and KING, A.I., (2007). "A Study of the Response of the Human Cadaver Head to Impact," J. Stapp Car Crash, 51, pp. 17-80.

HARDY, W.N., FOSTER, C., MASON, M., YANG, K., KING, A., and TASHMAN, S., (2001). "Investigation of Head Injury Mechanism Using Neutral Density Technology and High-Speed Biplanar X-ray," J. Stapp Car Crash, 45, pp. 337-368.

KALLIERIS, D., RIZZETTI, A., MATTERN, R., THUNNISSEN,J., and PHILIPPENS, M., (1996). "Cervical Human Spine Loads During Traumatomechanical Investigations," IRCOBI Conference, pp. 89-106.

LAUGHLIN, D.R., (1989). "A magnetohydrodynamic angular motion sensor for anthropomorphic test device instrumentation," J. Stapp Car Crash, 33, SAE Paper 892428.

KRIEGER, K.W., PADGAONKAR, A.J., and KING, A.I., (1976). "Full-scale experimental simulation of pedestrian-vehicle impacts," J. Stapp Car Crash, 20, SAE Paper 760813.

MARTIN, P.G., HALL, G.W., CRANDALL, J.R., PILKEY, W.D., CHOU, C.C., and FILETA, B.B., (1997). "Measurement Techniques for Angular Velocity and Acceleration in an Impact Environment," SAE Paper No. 970575, pp. 49-54.

MARTIN, P.G., HALL, G.W., CRANDALL, J.R., and PILKEY, W.D., (1998). "Measuring the Acceleration of a Rigid Body," Shock and Vibration 5, pp. 211-224.

NIKRAVESH, P.E., WEHAGE R.A., and KWON O.K., (1985). "Euler Parameters in Computational Kinematics and Dynamics," J. Mechanisms, Transmissions, and Automation in Design, 107, pp. 358-369.

NIKRAVESH, P. E. (1988). Computer-Aided Analysis of Mechanical Systems. Prentice-Hall: London.

NUSHOLTZ, G.S., KAIKER, P.S., and LEHMAN, R.J.,(1986). "Critical limitations on significant factors in head injury research," J. Stapp Car Crash, 30, SAE Paper 861890.

NUSHOLTZ, G.S., (1993). “Geometric Methods in Determining Rigid-body Dynamics,” Experimental Mechanics, 33, pp.153-158.

PADGAONKAR, A.J., KRIEGER, K.W., and KING, A.I., (1975). “Measurement of Angular Acceleration of a Rigid Body Using Linear Accelerometers,” J. Applied Mechanics 42, pp. 552-556.

SAE, (2007). Instrumentation for impact test, Part 1: Electronic instrumentation, SAE J211/1, Society of Automotive Engineers.

TAKHOUNTS, E.G., EPPINGER, R.H., CAMPBELL, J.Q., TANNOUS, R.E., POWER, E.D., and SHOOK, L.S., (2003). “On the Development of the SIMon Finite Element Head Model,” J. Stapp Car Crash, 47, SAE Paper No. 2003-22-0007.

VIANO, D.C., MELVIN, J.W., MCCLEARY, J.D., MADEIRA, R.G., SHEE, T.R., and HORSCH, J.D., (1986). "Measurement of head dynamics and facial contact forces in the Hybrid III dummy," J. Stapp Car Crash, 30, SAE Paper 861891

YOGANANDAN, N., PINTAR, F., STEMPER, B., SCHLICK, M., PHILIPPENS, M., and WISMANS, J., (2000). “Biomechanics of Human Occupants in Simulated Rear Crashes: Documentation of Neck Injuries and Comparison of Injury Criteria,” J. Stapp Car Crash, 44, SAE Paper No. 2001-01-SC14.

YOGANANDAN, N., ZHANG, J., PINTAR F.A., and LIU, Y.K., (2006). “Lightweight Low-Profile Nine-Accelerometer Package to Obtain Head Angular Accelerations in Short-Duration Impacts. J. Biomech. 39, pp. 1347-1354.

APPENDIX A

Coordinate transformation matrix ($\underline{\mathbf{A}}$) using 2-1-3 Euler angles (φ - θ - σ)

Transformation matrices for each of the Euler angles, φ, θ, and σ can be defined as in Equations (A1), (A2), and (A3), respectively:

$$\underline{\mathbf{B}} = \begin{bmatrix} \cos\varphi & 0 & \sin\varphi \\ 0 & 1 & 0 \\ -\sin\varphi & 0 & \cos\varphi \end{bmatrix} \tag{A1}$$

$$\underline{\mathbf{C}} = \begin{bmatrix} 1 & 0 & 0 \\ 0 & \cos\theta & -\sin\theta \\ 0 & \sin\theta & \cos\theta \end{bmatrix} \tag{A2}$$

$$\underline{\mathbf{D}} = \begin{bmatrix} \cos\sigma & -\sin\sigma & 0 \\ \sin\sigma & \cos\sigma & 0 \\ 0 & 0 & 1 \end{bmatrix} \tag{A3}$$

The transformation matrix, $\underline{\mathbf{A}}$, can then be determined as:

$$\underline{\mathbf{A}} = \underline{\mathbf{B}}\underline{\mathbf{C}}\underline{\mathbf{D}};$$

$$\underline{\mathbf{A}} = \begin{bmatrix} \cos\varphi\cos\sigma + \sin\varphi\sin\theta\sin\sigma & -\cos\varphi\sin\sigma + \sin\varphi\sin\theta\cos\sigma & \sin\varphi\cos\theta \\ \cos\theta\sin\sigma & \cos\theta\cos\sigma & -\sin\theta \\ -\sin\varphi\cos\sigma + \cos\varphi\sin\theta\sin\sigma & \sin\varphi\sin\sigma + \cos\varphi\sin\theta\cos\sigma & \cos\varphi\cos\theta \end{bmatrix} \tag{A4}$$

Updating the time-dependent transformation matrix using 2-1-3 Euler angles

Equation (2) can be differentiated with respect to time to obtain the velocity equation:

$$\dot{\underline{\mathbf{r}}}^{\mathbf{P}} = \dot{\underline{\mathbf{r}}} + \dot{\underline{\mathbf{A}}}\underline{\mathbf{s}}'^{\mathbf{P}} + \underline{\mathbf{A}}\dot{\underline{\mathbf{s}}}'^{\mathbf{P}} \tag{A5}$$

The third term in Equation (A5) is zero for a rigid body. By substituting $\underline{\mathbf{s}}'^{\mathbf{P}} = \underline{\mathbf{A}}^{\mathbf{T}}\underline{\mathbf{s}}^{\mathbf{P}}$, Equation (A5) can be written as:

$$\dot{\underline{\mathbf{r}}}^{\mathbf{P}} = \dot{\underline{\mathbf{r}}} + \dot{\underline{\mathbf{A}}}\underline{\mathbf{A}}^{\mathbf{T}}\underline{\mathbf{s}}^{\mathbf{P}} \tag{A6}$$

Equation (A6) is equivalent to the equation $\dot{\underline{\mathbf{r}}}^{\mathbf{P}} = \dot{\underline{\mathbf{r}}} + \underline{\boldsymbol{\omega}} \times \underline{\mathbf{s}}^{\mathbf{P}}$, where $\underline{\boldsymbol{\omega}}$ is the angular velocity of the body-fixed coordinate system relative to the global coordinate system. This equation can be written in matrix form as:

$$\dot{\underline{\mathbf{r}}}^{\mathbf{P}} = \dot{\underline{\mathbf{r}}} + \tilde{\underline{\boldsymbol{\omega}}}\underline{\mathbf{s}}^{\mathbf{P}} \tag{A7}$$

where: the tilda represents the cross product.

It is clear from Equations (A6) - (A7) that $\underline{\tilde{\boldsymbol{\omega}}} = \underline{\dot{\mathbf{A}}\mathbf{A}^{\mathrm{T}}}$. If $\underline{\tilde{\boldsymbol{\omega}}'}$ is the angular velocity with respect to the body fixed coordinate system, then the well known relationship between $\underline{\tilde{\boldsymbol{\omega}}}$ and $\underline{\tilde{\boldsymbol{\omega}}'}$ (i.e, $\underline{\tilde{\boldsymbol{\omega}}} = \underline{\mathbf{A}\tilde{\boldsymbol{\omega}}'\mathbf{A}^{\mathrm{T}}}$) can be used to obtain:

$$\underline{\mathbf{A}\tilde{\boldsymbol{\omega}}'\mathbf{A}^{\mathrm{T}}} = \underline{\dot{\mathbf{A}}\mathbf{A}^{\mathrm{T}}} \tag{A8}$$

It is then easy to show that:

$$\underline{\tilde{\boldsymbol{\omega}}'} = \underline{\mathbf{A}^{\mathrm{T}}}\,\underline{\dot{\mathbf{A}}} \tag{A9}$$

where: $\underline{\tilde{\boldsymbol{\omega}}'}$ is measured directly from the angular rate sensors in the 6aω and 3aω schemes (or determined from numerical integration of angular acceleration in the NAP scheme).

Equation (A9) can now be utilized to determine the relationship between the angular velocity with respect to the body fixed coordinate system and the angular velocity of the Euler angles with respect to the global coordinate system:

$$\begin{aligned}\underline{\tilde{\boldsymbol{\omega}}'} &= \underline{\mathbf{A}^{\mathrm{T}}}\,\underline{\dot{\mathbf{A}}} = \underline{(\mathbf{BCD})^{\mathrm{T}}}\,\underline{(\dot{\mathbf{B}}\mathbf{C}\mathbf{D} + \mathbf{B}\dot{\mathbf{C}}\mathbf{D} + \mathbf{B}\mathbf{C}\dot{\mathbf{D}})} \\ &= \underline{\mathbf{D}^{\mathrm{T}}}\,\underline{\mathbf{C}^{\mathrm{T}}}\,\underline{\mathbf{B}^{\mathrm{T}}}\,\underline{\dot{\mathbf{B}}\mathbf{C}\mathbf{D}} + \underline{\mathbf{D}^{\mathrm{T}}}\,\underline{\mathbf{C}^{\mathrm{T}}}\,\underline{\dot{\mathbf{C}}\mathbf{D}} + \underline{\mathbf{D}^{\mathrm{T}}}\,\underline{\dot{\mathbf{D}}}\end{aligned}$$

Thus:

$$\underline{\tilde{\boldsymbol{\omega}}'} = \begin{bmatrix} 0 & \dot{\varphi}\sin\theta - \dot{\sigma} & \dot{\varphi}\cos\theta\cos\sigma - \dot{\theta}\sin\sigma \\ -\dot{\varphi}\sin\theta + \dot{\sigma} & 0 & -\dot{\varphi}\cos\theta\sin\sigma - \dot{\theta}\cos\sigma \\ -\dot{\varphi}\cos\theta\cos\sigma + \dot{\theta}\sin\sigma & \dot{\varphi}\cos\theta\sin\sigma + \dot{\theta}\cos\sigma & 0 \end{bmatrix} \tag{A10}$$

$\underline{\tilde{\boldsymbol{\omega}}'}$ can also be written as:

$$\underline{\tilde{\boldsymbol{\omega}}'} = \begin{bmatrix} 0 & -\omega_z' & \omega_y' \\ \omega_z' & 0 & -\omega_x' \\ -\omega_y' & \omega_x' & 0 \end{bmatrix} \tag{A11}$$

Equations (A10) and (A11) can then be equated and the time dependent angular velocities ($\dot{\varphi}$, $\dot{\theta}$, and $\dot{\sigma}$) of the 2-1-3 Euler angles obtained using Equations (A12) and (A13).

$$\begin{bmatrix} \omega_x' \\ \omega_y' \\ \omega_z' \end{bmatrix} = \begin{bmatrix} \cos\theta\sin\sigma & \cos\sigma & 0 \\ \cos\theta\cos\sigma & -\sin\sigma & 0 \\ -\sin\theta & 0 & 1 \end{bmatrix} \begin{bmatrix} \dot{\varphi} \\ \dot{\theta} \\ \dot{\sigma} \end{bmatrix} \tag{A12}$$

$$\begin{bmatrix} \dot{\varphi} \\ \dot{\theta} \\ \dot{\sigma} \end{bmatrix} = \begin{bmatrix} \cos\theta\sin\sigma & \cos\sigma & 0 \\ \cos\theta\cos\sigma & -\sin\sigma & 0 \\ -\sin\theta & 0 & 1 \end{bmatrix}^{-1} \begin{bmatrix} \omega_x' \\ \omega_y' \\ \omega_z' \end{bmatrix} \tag{A13}$$

The Euler angles at each subsequent time step can then be determined by numerically integrating the angular velocities of the Euler angles using Equation (A14):

$$\begin{aligned} \varphi_{i+1} &= \varphi_i + 0.5 \times (\dot{\varphi}_i + \dot{\varphi}_{i+1}) \times \Delta t \\ \theta_{i+1} &= \theta_i + 0.5 \times (\dot{\theta}_i + \dot{\theta}_{i+1}) \times \Delta t \\ \sigma_{i+1} &= \sigma_i + 0.5 \times (\dot{\sigma}_i + \dot{\sigma}_{i+1}) \times \Delta t \end{aligned} \tag{A14}$$